JAMES | Journal of Advances in Modeling Earth Systems

RESEARCH ARTICLE
10.1029/2019MS001828

Interactions Between the Amazonian Rainforest and Cumuli Clouds: A Large-Eddy Simulation, High-Resolution ECMWF, and Observational Intercomparison Study

J. Vilà-Guerau de Arellano[1,2], X. Wang[1], X. Pedruzo-Bagazgoitia[1], M. Sikma[1], A. Agustí-Panareda[3], S. Boussetta[3], G. Balsamo[3], L. A. T. Machado[4,5], T. Biscaro[4], P. Gentine[6], S. T. Martin[7], J. D. Fuentes[8], and T. Gerken[8]

[1]Meteorology and Air Quality Section, Wageningen University, Wageningen, Netherlands, [2]Atmospheric Chemistry Department, Max Planck Institute for Chemistry, Mainz, Germany, [3]European Centre for Medium-Range Forecast, Reading, UK, [4]Centro de Previsao de Tempo e Estudios Climaticos, INPE, Sao Jose dos Campos, Brasil, [5]Multiphase Chemistry Department, Max Planck Institute for Chemistry, Mainz, Germany, [6]Earth and Environmental Engineering, Columbia University, New York, NY, USA, [7]Department of Earth and Planetary Sciences, Harvard University, Cambridge, MA, USA, [8]Department of Meteorology and Atmospheric Science, The Pennsylvania State University, University Park, PA, USA

Key Points:
- Explicit interactions between carbon uptake and clouds on subdaily and subkilometer scales are modeled and validated
- NEE observations show an early afternoon shift from a CO_2 sink to a source, whereas in the model results, the CO_2 uptake is longer
- Observations and DALES results show enhancement of moisture transport at cloud base that favors triggering afternoon deep convection

Correspondence to:
J. Vilà-Guerau de Arellano,
jordi.vila@wur.nl

Citation:
Vilà-Guerau de Arellano, J., Wang, X., Pedruzo-Bagazgoitia, X., Sikma, M., Agusti-Panareda, A., Boussetta, S., et al. (2020). Interactions between the Amazonian rainforest and cumuli clouds: A large-eddy simulation, high-resolution ECMWF, and observational intercomparison study. *Journal of Advances in Modeling Earth Systems*, *12*, e2019MS001828. https://doi.org/10.1029/2019MS001828

Received 22 JUL 2019
Accepted 24 APR 2020
Accepted article online 29 APR 2020

Abstract The explicit coupling at meter and second scales of vegetation's responses to the atmospheric-boundary layer dynamics drives a dynamic heterogeneity that influences canopy-top fluxes and cloud formation. Focusing on a representative day during the Amazonian dry season, we investigate the diurnal cycle of energy, moisture and carbon dioxide at the canopy top, and the transition from clear to cloudy conditions. To this end, we compare results from a large-eddy simulation technique, a high-resolution global weather model, and a complete observational data set collected during the GoAmazon14/15 campaign. The overall model-observation comparisons of radiation and canopy-top fluxes, turbulence, and cloud dynamics are very satisfactory, with all the modeled variables lying within the standard deviation of the monthly aggregated observations. Our analysis indicates that the timing of the change in the daylight carbon exchange, from a sink to a source, remains uncertain and is probably related to the stomata closure caused by the increase in vapor pressure deficit during the afternoon. We demonstrate quantitatively that heat and moisture transport from the subcloud layer into the cloud layer are misrepresented by the global model, yielding low values of specific humidity and thermal instability above the cloud base. Finally, the numerical simulations and observational data are adequate settings for benchmarking more comprehensive studies of plant responses, microphysics, and radiation.

Plain Language Summary Clouds and forest in the Amazonian rainforest region are closely related. We investigated the final month of the Amazonian dry season in order to study interactions between the rainforest and the overlying atmosphere, placing particular emphasis on studying small spatiotemporal effects, such as that of cloud shading on photosynthesis. We employed three different methods: a cloud-turbulence resolving model, a global weather model, and a complete set of canopy-top and atmospheric observations. We holistically studied these relationships by systematically analyzing the characteristics of incoming solar radiation, evapotranspiration, and cloud cover and thickness. This comparison enabled us to make two relevant findings related to these diurnal carbon and cloud cycles. First, we observed that photosynthesis is offset by the soil carbon dioxide efflux earlier than the two models calculations. With respect to cloud formation and intensification, we showed quantitatively that the inefficiently modeled moisture transport leads to less active shallow convection, which may be insufficient to trigger deep convection. This systematic study paves the way for more comprehensive studies that would include more complex descriptions of microphysics processes and radiation, as well as chemistry and aerosol formation.

1. Introduction

Two of the most important uncertainties in climate studies are associated with the impact of clouds on radiative transfer (Schneider et al., 2017; Zelinka et al., 2017) and the terrestrial carbon dioxide (CO_2) sink (Le Quéré et al., 2009). These uncertainties are typically quantified by global circulation models (Vial et al., 2013). However, due to their simplified physical representation and interaction, such models have difficulty in attributing the change to uncertainties to specific processes and their interactions occurring at regional level. The Amazonian tropical forest is one region in which the wide range of spatiotemporal characteristics of cloud dynamics interacts with the terrestrial CO_2 sink. Previous studies have demonstrated the need to study short-term and rapid spatiotemporal perturbations to quantify new insights into the diurnal clouds and carbon cycles. More specifically, photosynthesis and stomatal aperture responses to radiative perturbations influence (i) the surface energy balance (Doutriaux-Boucher et al., 2009; Pedruzo-Bagazgoitia et al., 2017; Sikma et al., 2018), (ii) key length scales of clouds such as their horizontal size and cloud separation (Horn et al., 2015), and (iii) cloud transport properties (Sikma & Vilà-Guerau de Arellano, 2019). In reproducing these couplings, the model's representation of the radiative transfer at the canopy top perturbed by clouds plays a key role (Jakub & Mayer, 2017).

In order to understand the coupling between the Amazonian tropical forest and the overlying atmosphere, we here investigate the myriad links that exist between convective boundary-layer clouds and the responses of the tropical forest to rapid, subdaily and subkilometer perturbations of radiation and the state of meteorological variables such as temperature or water vapor deficit. Our approach is to explicitly solve the coupling between radiation perturbation by clouds and vegetation responses, and their subsequent influence on turbulent transport and intensity. The fact that biochemical and physical local processes are not yet fully integrated in large-scale modeling studies limits our understanding of the concatenation of biochemical and physical processes that occur between the canopy and the atmosphere. We therefore aim here to solve and observe such processes on the temporal and length scales on which they occur and interact (Schneider et al., 2017).

Our study extends comparative efforts led by Working Group 1 (WG-1) of the GCCS (GEWEX, Global Energy Water Cycle Experiment) cloud system study (Browning, 1993). Although studies based on the simulation of cumuli over land already exist (Brown et al., 2002; Lenderink et al., 2004), they omit interactions with the surface and are based on limited observations. The analysis of the diurnal carbon cycle enables us to connect with current initiatives that aim to improve the quantification of the net CO_2 sources and sinks in the Amazonian basin on seasonal scales (van der Laan-Luijkx et al., 2015).

Figure 1 guides the reader through the processes of simulation, validation, and analysis employed in this study. We begin by discussing how radiation perturbation, influenced by the presence of clouds and canopy, affects the assimilation of CO_2 and stomatal aperture (Figure 1, left). Net ecosystem exchange observations above the canopy enable us to determine whether the partition of canopy CO_2 assimilation and soil efflux is adequately represented by current state-of-the-art models. Here, we assume that plants optimize their CO_2 assimilation by actively limiting their rate of water loss to improve the efficiency of their water use. To this end, we establish a link between the diurnal carbon cycle and those for water and energy. The interconnection diagram shows that variations in surface-energy balance partitioning into sensible and latent heat fluxes lead to changes in the turbulent transport of momentum, heat, and moisture and therefore in the dynamics of the boundary layer. We therefore study how the vertical profiles of wind, potential temperature, specific humidity, and CO_2 depend on these local canopy-top turbulent fluxes and lead to changes on the vertical thermodynamic structure. Finally, the transport of momentum, heat, and moisture drives the onset of clouds, their intensity, and their final dissipation or evolution to deep convective clouds.

Our paper presents and discusses modeling results that reproduce an average day, based on observed monthly mean, that represents the dynamics of an atmospheric boundary layer developed above the Amazonian rainforest during the dry season. This particular day is characterized by shallow cumuli, and these clouds perturb both the incoming solar radiation and turbulence above the rainforest (Garstang & Fitzjarrald, 1999). The cumulative effect of these diurnal cycles in moistening and destabilizing the lower free troposphere in September is crucial to the transition season between dry to wet season (which normally starts in October) above the Amazonian tropical forest (Gentine et al., 2019; Wright et al., 2017). Our methodology is shown in Figure 1 (right panel). On the basis of a complete set of observations gathered

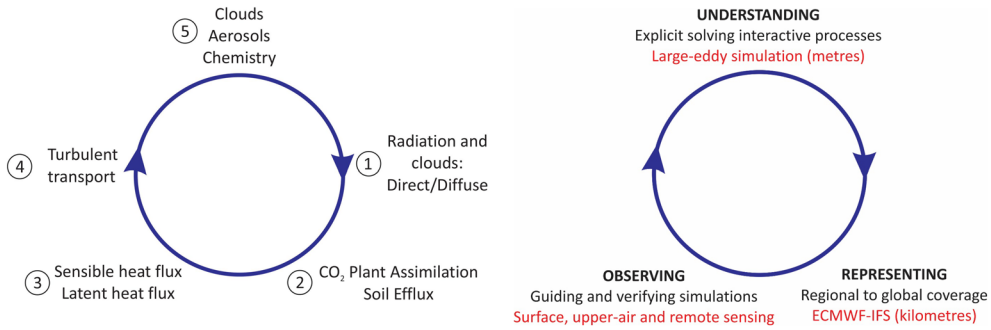

Figure 1. Left panel: overview of the processes studied. The numbers indicate the order of our analysis. Right panel: The methodological approach combines observations, large-eddy simulations numerical experiments (DALES), and a high-resolution global model (IFS) to reproduce a representative day during the Amazonian dry season. The experimental design is based on the data collected in September 2014 in central Amazonia as part of the GoAmazon campaign (Martin et al., 2016).

during the GoAmazon campaign 2014/2015 (Martin et al., 2016), we design a comprehensive numerical experiment that was performed by the Dutch Atmospheric Large Eddy Simulation (DALES), that is, subkilometer horizontal resolution of 53 m × 53 m (Ouwersloot et al., 2016).

The numerical experiments explicitly simulate the coupling between the canopy top, including plant responses, and radiation and turbulence perturbations. To complete the study, we include the results of numerical experiments from a high global weather model resolution (9 km × 9 km) of the European Centre for Medium-Range Weather Forecasts (ECMWF)-Integrative Forecasting System (IFS) (Balsamo et al., 2011; Boussetta et al., 2013) (from now on IFS). Our goal is to study differences between processes that are explicitly solved by DALES, such as clouds or turbulence, and a representation based on parametrizations as calculated by IFS. Regarding the biological descriptions, DALES and IFS represent plant photosynthesis and stomatal aperture by means of biophysical mechanistic model that employs similar assumptions regarding the dependences on photosynthetically active radiation, temperature, water vapor pressure deficit, and internal leaf carbon dioxide level (Calvet, 2000; Ronda et al., 2001).

Our objective is to understand the chain of diurnal land-atmosphere interactions in the Amazonian region and to assess how accurately the processes and their interactions are represented. We break down this objective into three aspects:

1. to quantify the ability of a turbulent resolving model (DALES) and a high-resolution large-scale global model (ECMWF-IFS) to reproduce the diurnal variability, spatial dynamic heterogeneity, and vertical dependence of the meteorological state variables and carbon dioxide, including the impact of boundary-layer clouds;
2. to explore the impact of resolving explicitly the coupling between vegetation and canopy. More specifically,
    a. to determine how radiation processes (cloud perturbations) and state variables (wind, water vapor pressure deficit, and temperature) control the subhourly variability of the net ecosystem exchange, gross primary production, and soil respiration and to relate these canopy-top vegetation responses to the sensible and latent heat fluxes.
    b. to quantify how heat and moisture are turbulently transported between the subcloud and cloud layers and the impact of these processes on the dynamic evolution of shallow cumuli;
3. to propose a well-evaluated numerical experiment case as a benchmark for further studies of how atmospheric radiation, turbulence, moist convection, microphysics, and chemistry interact with the tropical forest.

2. Research Design

We focus on the month of September 2014, which is at the end of the dry period in central Amazon (see Figure 2). The dry period is characterized by a transitional convective regime (Zhuang et al., 2017), during which deep convection can develop locally based on forest evapotranspiration dynamics and can influence the dry-wet seasonal transition (Wright et al., 2017). For the selected day (10 September 2014), we show the cloud spatial pattern by the Moderate Resolution Imaging Spectroradiometer MODIS and their

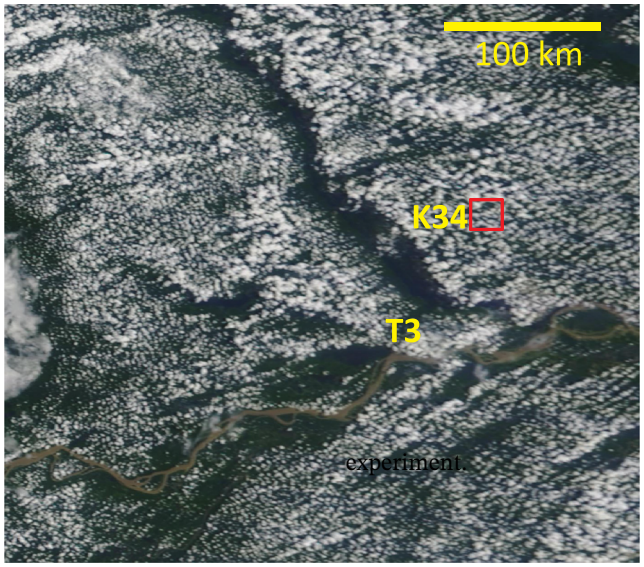

Figure 2. MODIS image displays the situation on 10 September 2014 at 15 hr and 7 min UTC (11 hr and 7 min LT). The image shows a representative day during the dry season, characterized by the presence of shallow cumulus streets. MODIS image: bottom left (−4.3°S, −62,5°W) and top right (−1.6°S, −59.5°W). The GoAmazon2014/15 sites K34 (T0k) and T3 are indicated. DALES domain (19,080 m × 19,080 m) is represented by the red square. For details on the location of the observations, see section 3.3.

potential impact on the perturbations on the radiation field and on surface processes in Figure 2. It shows a representative during the dry season in Amazonia, with a situation characterized by shallow convection organized in cloud streets. During this month, three aspects govern the interaction between the tropical forest and the overlying atmosphere: (a) The large-scale situation is characterized by Atlantic Ocean air masses coming from the northeast and east with typical trade wind profiles (see Figures 11 and 15); (b) these air masses are influenced by the regional surface and atmospheric conditions, above Amazon tropical forest conditions as they traverse the 1,500 km path from the ocean; and (c) the local conditions above the rainforest and in the atmospheric boundary layer. The combined effect of these three aspects impacts the wind, potential temperature, and specific humidity profiles (section 6) and is taken into account in the initial profile conditions of the large-eddy simulation experiment.

In the simulation the subdaily and subkilometer atmospheric flow by DALES, we assume the following. In this Amazonian region (west of Manaus in Brazil), the influence of the Atlantic Ocean conditions and the air mass traveling above the rainforest partly govern the thermodynamic profiles (Makarieva et al., 2014; Spracklen et al., 2012). The explicit influence of the large-scale synoptic forcing and the influence of secondary circulations induced by surface heterogeneities such as the presence of rivers (Burleyson et al., 2016) are only included in the initial profiles of these state variables and CO_2. Our research design focused on nonprecipitating shallow cumulus, with the primary aim of studying the coupling between evapotranspiration, the diurnal carbon cycle, and the atmospheric boundary layer conditions. We mainly focus on the transition between the clear to the cloudy boundary-layer and the early stages on shallow convection. We therefore quantify insights on conditions that can be optimal to preconditioning deep convection, but our focus remains on shallow cumuli. Although aerosols have not been explicitly treated here, they play a relevant role in controlling radiation and microphysics in this region (Feingold et al., 2005).

On research strategy is based on a comprehensive comparison of the representative DALES experiment with the complete data collected from GoAmazon2014/15 sites. In the design of the DALES numerical experiment, we assume the same canopy-top cover type as defined in Table A3 and the absence of land heterogeneities. The IFS, a high-resolution global model, results computed for the same location were used to assess how a highly parametrized model is able to reproduce this situation. IFS results are shown for the same day (10 September 2014). Compared to typical temporal output in global models, we show here results every 1 hr to evaluate more accurately the representation of the diurnal cycle.

From the observations, and using the two sites K34 and T3 shown in Figure 2 and introduced in section 3.3, we calculated a 1-day average aggregate from the monthly measurements in order to obtain additional information regarding the variability of the variable and how the maximum and minimum values vary during the day. By comparing the numerical experiments with an average day during the dry season, we attempted to move beyond the standard large-eddy simulation studies based on studying a single day and avoid gaps on the observations. Moreover, the observational-aggregated variables enable us to estimate how much each variable varies on the diurnal scale. Here, we consider a satisfactory agreement if all the modeled variables lie within the envelope of the monthly observed composite. In order to study the effect of using a monthly composite on model evaluation, we also include in the figures observations of a single day characterized by shallow cumuli. Due to the difficulty in selecting the data only characterized by shallow cumuli, we decides to use all the data available. In that respect our results are more representative of the transition between clear and boundary-layer cloud and the early stages of shallow cumuli maturation. After approximately 14 LT (local time LT is defined 4 hr after UTC), the monthly observational aggregation could show the development of deep convective clouds and cumuliform clouds. We placed special emphasis on the overall performance of the numerical experiment, following the processes and their interactions, as shown in Figure 1.

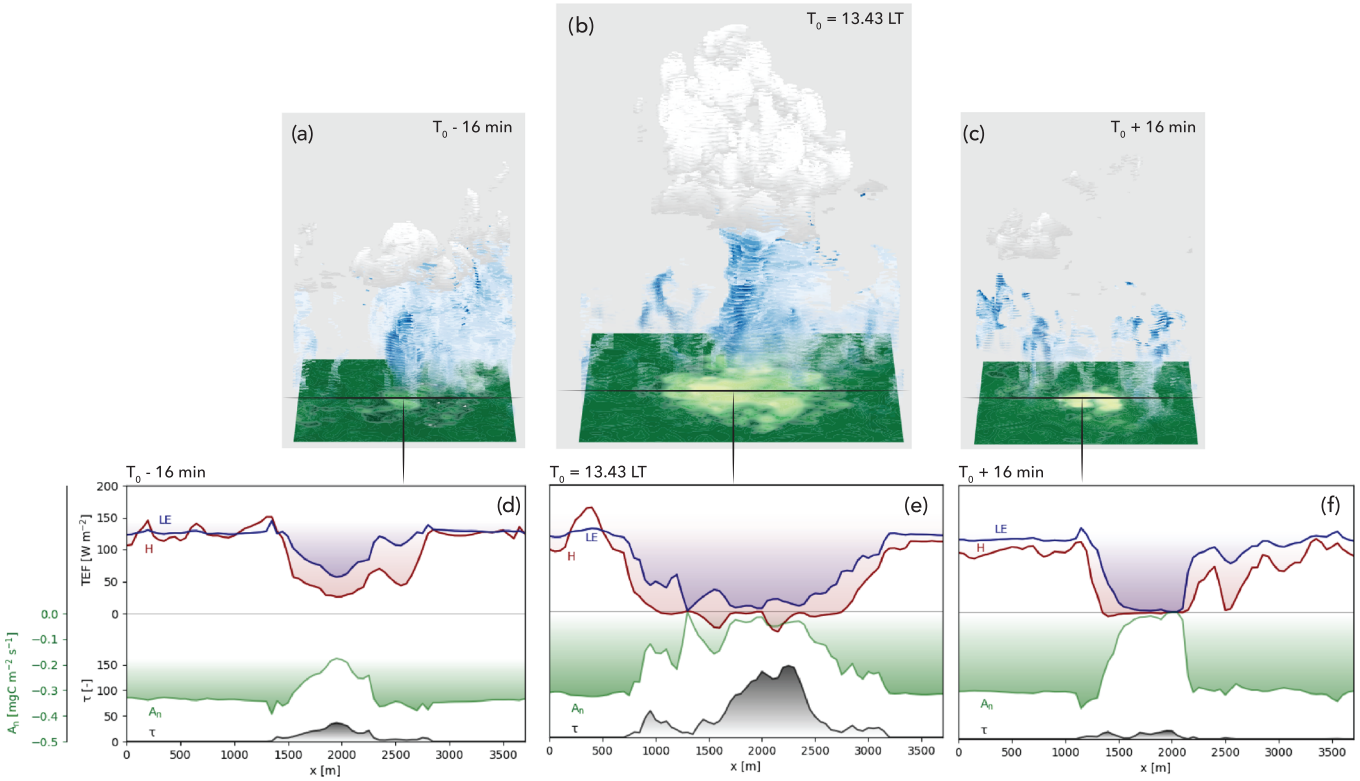

Figure 3. Top panel: three stages, around 13.43 LT (10 September), of a shallow cumulus cycle: (a) early formation, (b) maturity, and (c) dissipation. The x, y, and z axes are 4,000, 4,000, and 3,000 m, respectively. The blue color represents the specific humidity with maximum values of 5 $g_w\ kg_a^{-1}$. The green (more open stomata) to yellow (more close stomata) at the surface is the canopy of surface resistance, a representation of the stomatal aperture, with values ranging from 220 to 240 sm^{-1}. Bottom panel: At the surface, the impact of the cloud disturbances (radiation, cold temperatures, and water vapor deficit) on the energy (H in red, TEF: turbulent energy fluxes), moisture (LE in blue), and CO_2 assimilation (A_n in green) fluxes are shown at (d)–(f). Cloud thickness (gray) is quantified by the cloud optical depth (τ). The color shading is to improve the visualization.

3. Methods

3.1. Explicit Coupling of Radiation and Turbulence by DALES

The level of detail in simulating the evolving coupling between the shallow cumulus and the responses of the forest is shown in Figure 3. The cloud optical depth (τ) indicates the cloud opacity, and therefore its impact on photosynthetically active radiation (PAR), a main driver of photosynthesis. The dependence of the stomatal aperture on rapid changes in PAR enable us to study the modifications of the rates of assimilation of CO_2 due to rapid changes in the stomatal aperture (represented by the canopy resistance) and therefore to latent heat flux (LE). LE also depends on the temperature changes caused by cloud shading that yields shifts in the canopy top energy balance, and therefore on the sensible heat flux (SH). We call these rapid and short changes above the canopy "dynamic heterogeneity" (Horn et al., 2015). As shown by Sikma and Vilà-Guerau de Arellano (2019), dynamic heterogeneity alters both turbulent transport and cloud dynamics.

These numerical experiments were performed using the Dutch Atmospheric Large Eddy Simulation (DALES (Heus et al., 2010; Ouwersloot et al., 2016). Version 4.2 was used and can be downloaded online (at http://doi.org/10.5281/zenodo.3759193). For this study, and following Figure 1, we show in Table A1 the processes employed in the study and their physical representation. In short, we prescribe horizontal grid cells of 53 m × 53 m with a 20-m vertical resolution in a domain near the observational site (see Figure 2). We prescribe this relatively coarse vertical resolution in DALES in order to facilitate comparison with the global model (section 3.2). The Rapid Radiative Transfer Model for Global circulation model (RRTMG) (Iacono et al., 2008), a one-dimensional radiative model, calculates the impact of clouds in partitioning and modifying direct and diffuse radiation. The radiative transfer is calculated independently at each column and with the same time step as the dynamics (the time step is variable but has a maximum value

of 1 s). Consequently, we obtain, at each column, a different amount of direct and diffuse PAR that leads to different responses of the stomatal aperture and photosynthesis. In our numerical experiments, we assume an instantaneous response of the stomatal aperture and photosynthesis to these cloud modifications of PAR. Although the stomatal aperture time lag and background wind play key roles in the coupling between vegetation and boundary-layer clouds (Sikma et al., 2018), by assuming an instantaneous stomatal aperture response to radiation perturbations, our DALES experiments are characterized by the strongest coupling between cloud shading and stomatal aperture. We also assume that the canopy is a bulk layer represented by unique values for the temperature and specific humidity, as these evolve through time. Within this bulk canopy layer, we represent the transfer of radiation within the canopy by the two-big leaves (one sunlit and the other shaded) approach in order to take into account the different responses to sunlit and shaded conditions (Pedruzo-Bagazgoitia et al., 2017). In this formulation, we calculated two different vertical extinction profiles of direct and diffuse radiation. The radiation transfer in the canopy is important because it influences the plant CO_2 assimilation and therefore the plant transpiration at canopy level. The coupling between the forest and the atmospheric conditions is modeled with the A-gs scheme (CO_2 assimilation-stomatal conductivity), which represents the evolution of stomatal aperture and photosynthesis in the course of the day. This model is described at Jacobs and de Bruin (1997) and Ronda et al. (2001). The A-gs model is a semiempirical physiological model linking the leaf photosynthesis rate, the net assimilation of CO_2, and the leaf conductance to external, surface, and atmospheric factors (e.g., soil moisture, net radiation, air temperature, and air humidity). To calculate the net ecosystem exchange (NEE), we also compute the soil efflux following Jacobs et al. (2007). This heterotrophic respiration depends on the temperature of the soil in contact with the atmosphere and the soil moisture stress. The coupling between the plant and atmospheric conditions in both models is made throughout the variations in plant transpiration via the stomatal aperture regulation (Katul et al., 2012). The plant responses thus influence how the net available radiation is partitioned between the sensible and latent heat fluxes. In DALES, all these radiation-surface-dynamic couplings are calculated simultaneously every second for each grid cell.

The numerical settings, including the initial profiles of the thermodynamic state variables in the entire Amazonian boundary layer, are presented in Table A2. The initial profiles are inspired by the radiosonde readings launched at 1.30 LT (5.30 UTC). Plant and soil boundary conditions can be found in Table A3. The soil temperature and soil moisture at the four depths were prescribed and constrained based on the best comparison with the canopy-top fluxes of momentum, heat, moisture, and the net ecosystem exchange. Table A3 is completed by the constants used in the plant physiology model to calculate photosynthesis and stomata aperture values (Table A4). It is worth to noting that large-scale forcings such as vertical subsidence of advection of momentum, heat, moisture, and CO_2 are not included in the numerical experiment, which focuses only on the rainforest and atmosphere interactions.

3.2. High-Resolution Global Calculations by IFS

For the same month, we calculated the weather and its coupling to the canopy top by means of the European Centre Medium-Range Weather Forecast- Integrated Forecasting System (IFS). The horizontal resolution is approximately 9 km × 9 km. In the vertical plane, 137 vertical levels are defined, that is, with a resolution in the atmospheric boundary layer similar to DALES of approximately 20 m. In this study, which is based on the IFS cycle CY45R1, runs for 2 days (9–10 September 2014) are performed, where only the second day's results are considered. The frequency of the output is hourly. This simulation is initialized with the operational IFS archive, the radiation transfer is calculated every hour, and in this experiment, the full A-gs based model is switched on for both CO_2 fluxes and evapotranspiration. Note that this is a slightly different configuration from the operational IFS. In this study we represent both plant transpiration and CO_2 assimilation with the A-gs scheme, whereas in the operational IFS plant transpiration is calculated using the Jarvis-Stewart representation. In relation to the IFS performance with high resolution, it should be noted that in general, the high-resolution deterministic simulations have an equivalent performance to the low-resolution ensemble simulations. A full validation of the IFS system is beyond the scope of this paper; however, more detailed evaluation of the IFS CY45R1 cycle could be found in Buizza et al. (2018) (for more information see www.ecmwf.int/en/forecasts/documentation-and-support/changes-ecmwf-model/ifs-documentation).

Figure 4 shows the net ecosystem exchange and the cloud cover (low clouds) calculated by IFS as an example of the spatial variability over the Amazonian region and a close-up (right figures) of the region under study to show the level of detail in representing the sources/sinks of NEE and cloud cover. Due to our interest in

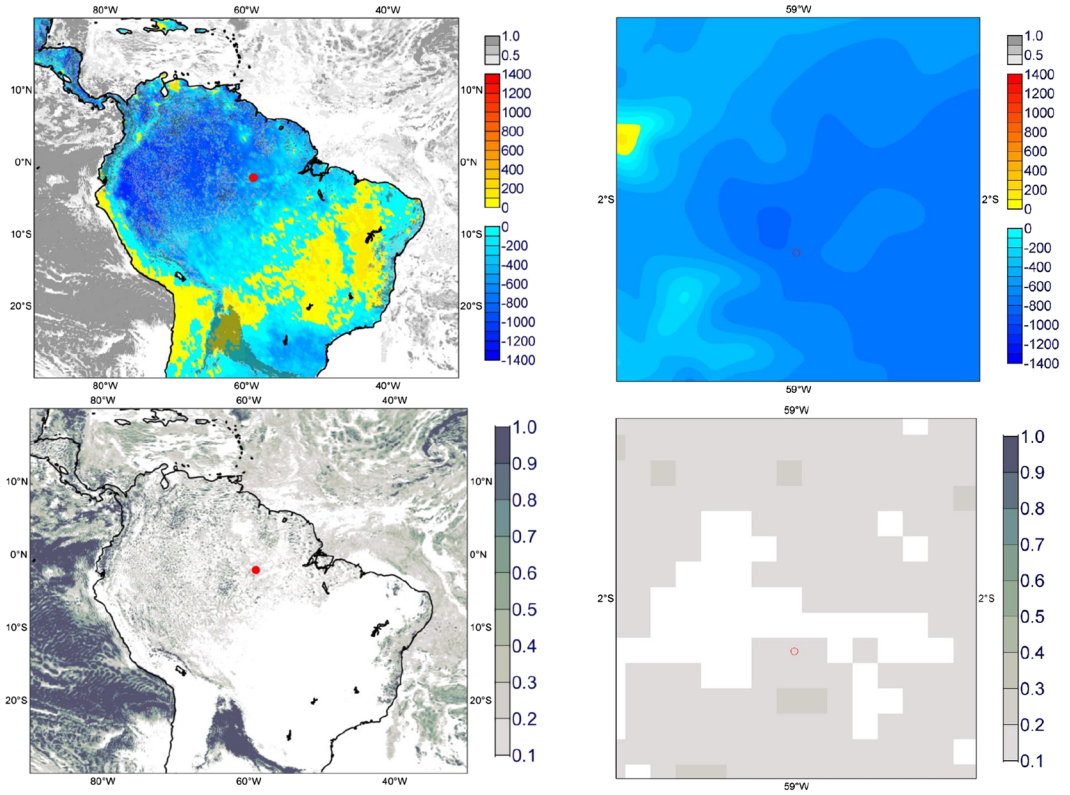

Figure 4. Top panel: IFS models results of the accumulated (from 15 to 18 UTC) net ecosystem exchange in units g m^{-2} day^{-1} of the entire Amazonian basin (left) and zoom in to the simulated domain (right) (see Figure 2). Color bars: Negative and positive values represent a sink and a source of the net exchange ecosystem CO_2, respectively. White-black bars represent the cloud cover ranging from 0 to 1. Bottom panel: IFS model results of low cloud cover (from 0 to 1) of the entire Amazonian basin (left) and a close-up of the simulated region (right). The variables correspond to 10^{th} September 2014. The circle marks the DALES domain and the K34 (T0k) site of the GoAmazon2014/15 experiment.

studying the land-atmosphere coupling, the IFS modeling was performed using the CTESSEL land-surface representation (Boussetta et al., 2013). CTESSEL is based on the IFS land-surface model HTESSEL (Balsamo et al., 2011), but it represents mechanistically the CO_2 plant and soil exchanges unlike HTESSEL. Like DALES, this coupling is modeled using the same biophysical model A-gs, but with a modified version of the effects of soil water stress on photosynthesis and canopy resistance (Calvet et al., 1998; Calvet, 2000). A reference respiration parameter for each vegetation type was used to simulate the heterotrophic respiration without direct simulation, and there was no direct simulation of the individual carbon pools. The reference values were obtained by optimization with respect to flux measurements for the different types of vegetation. The optimization of the CO_2 model was performed in an off-line simulation over the eddy-covariance sites grouped by plant functional type. The optimized parameters (mesophyl conductance and ecosystem respiration) were found by minimizing the root mean square error (RMSE) between observed and simulated CO_2 fluxes. For each site within the same vegetation type group, the optimized parameters were allowed to vary within a fixed range chosen from the literature. The ecosystem respiration was then obtained through a functional relationship that depends on soil moisture and surface temperature. A detailed description and evaluation of the CTESSEL model can be found in Boussetta et al. (2013). The atmospheric CO_2 simulations were generated using the Copernicus Atmosphere Monitoring Service (CAMS) forecasting system based on the IFS model at 9 km as documented by Agustí-Panareda et al. (2019). The synergy between CO_2 fluxes modeled by CTESSEL and the tracer transport has been shown to improve the CO_2 forecast skill at synoptic scales (Agustí-Panareda et al., 2014). In order to be consistent with DALES, we took 10 September 2014 as the representative day to be compared. The location selected is the grid point near the K34 tower (see section 3.3), and the frequency of the output was every 1 hr.

3.3. Canopy-Top and Upper-Atmospheric Observations During GoAmazon2014/15

From the GoAmazon2014/15 campaign, we also select the dry month of September 2014, that is, precipitation below 150 mm. The observations employed for the evaluation were collected at two sites: (a) the K34 site or T0k site of GoAmazon2014/5 (−2.6091°, −60.2093°) (Fuentes et al., 2016) and (b) and the T3 site (−3.2133°, −60.5987°) (Martin et al., 2016) (see Figure 2). The two observation sites were separated by approximately 80 km. The canopy-top observations at the T0k that were taken at 48.2 m (approximately 13 m above the canopy) include the shortwave and longwave (upward and downward) components of radiation. Unfortunately, there were no data available on the direct and diffuse radiation. The canopy-top turbulent fluxes include friction velocity u_*, net evapotranspiration or latent heat flux and sensible heat flux, and NEE observed at 30-min intervals (Fuentes et al., 2016). The data were complemented with the CO_2 mixing ratio measurements. It should be noted that canopy height at T0k is around 35 m. The canopy is dense up to about 30 m and then becomes sparser, with the highest tree reaching 35 m.

A key aspect of the study was the combination of the canopy-top data with upper-atmospheric measurements. For this purpose, we used the evolution of the thermodynamic profiles at T3: potential temperature, specific humidity, and the two components of the horizontal velocity. The launch times were 11.30 UTC (07.30 LT), 14.30 UTC (10.30 LT), 17.30 UTC (13.30 LT), and 23.30 (19.30 LT). Each sounding, launched at T3, takes approximately 15 min to profile the 4,000 m analyzed in our study. Remotely sensed cloud characteristics including fraction, base, and top height were estimated by combining the ARM Lidar, W-band radar, and ceilometer data (Giangrande et al., 2017). The in situ and remote sensing observations were made at the same location. Cloud fraction was computed as the percentage of the time when any cloud base was below the height at which freezing temperature was detected. Cloud base was calculated as the average height of clouds at each point averaged in time. The 95 GHz W-band ARM cloud radar (WACR) was employed to estimate the cloud top. Cloud masking was computed according to the active remote cloud sensing of clouds methodologies described by Clothiaux et al. (2000). Cloud-base, top, and cover measurements were averaged over 1 hr. The W band was only available on 1 to 13 and 29 to 30 September.

4. Radiation and Turbulent Fluxes above the Tropical Forest

Figure 5 shows the observed net available radiation and its representation by DALES and IFS. First, we focus on the large decrease in the minimum value of the monthly composite of the net available radiation Qn (defined as the net budget of the two shortwave and two longwave radiative components) just before 12 LT. It enables us to distinguish two regimes marked by the appearance of clouds that become thicker over time. Before this point in time, DALES slightly overestimates the net available radiation Qn compared to the monthly average observations and IFS results. After 12 LT, DALES and IFS clear-sky net radiation values slightly overestimated the monthly observation whereas the IFS net radiation values (blue squares) underestimate it, which can be related to the representation of thicker cloud. The 10 September observations (blue circles) show the effect of the shallow cumulus reflection quantified by higher values than the clear sky ones.

Before we compare our observations with the model results, it is necessary to discuss the plausible explanations for discrepancies in Q_n due to the contributions of shortwave and longwave radition. First, and regarding the net shortwave radiation, it has been observed by Giambelluca et al. (1997) that the Amazonian tropical forest albedo ranges during in the morning hours (until approximately 11 LT) from values higher than 0.20 down to 0.15. This range of variation applies to vegetation of all ages. DALES employs a constant value of 0.15. Second, and regarding the longwave radiation, the coarse representation of the interface between the tall canopy forest and the atmosphere in both models may lead to higher temperature estimates due to the omission of turbulent mixing between the lower potential temperatures within the canopy and the higher temperatures during the day (Fitzjarrald et al., 1990). A more physical representation of turbulent mixing in DALES between the in canopy state variables and the above canopy might improve the coupling at the interface between the canopy and roughness sublayer as was inferred from Amazonian rainforest observations by Freire et al. (2017). Therefore, we attribute these higher values of the outgoing longwave radiation to this overestimation of the DALES canopy-top temperature. The higher temperatures are due to the absence of mixing of the cold air within the canopy. Finally, and as a result of the initial settings, DALES is unable to simulate the radiative disturbances due to low clouds conditions just above the canopy that have been reported by Anber et al. (2015). Similar low-cloud conditions are also evident

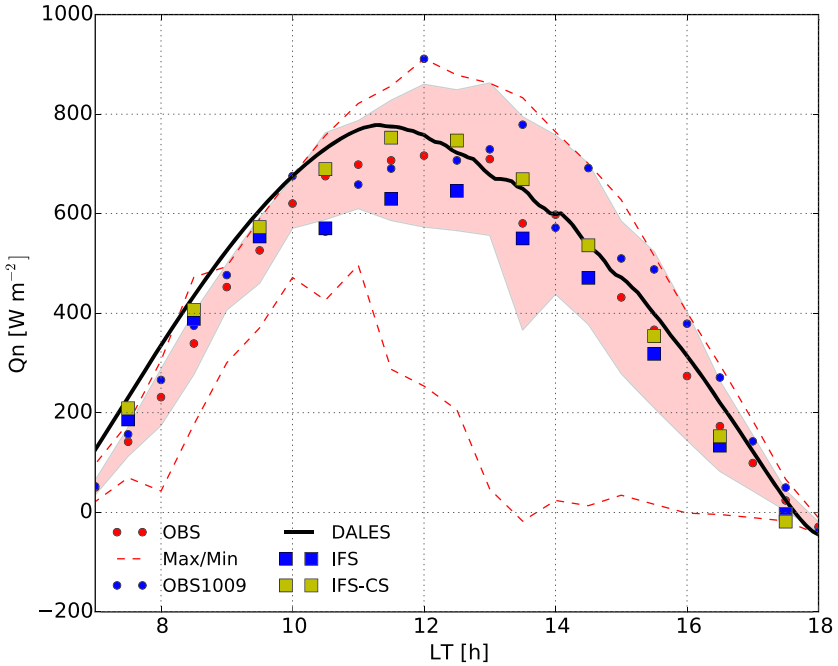

Figure 5. The observed and simulated available net radiation energy (Qn). Observations (mean, standard deviation, and maximum and minimum) refer to the entire month of September 2014, collected during the GoAmazon2014/15 campaign. Observations were made above the canopy at the T0 Ksite. OBS1009 stands for the observations made on 10 September 2014. The DALES and IFS results are from 10 September 2014. IFS-CS represents the net available radiation under clear-sky conditions.

in the observations in the IFS results, which report cloud cover during the night-day transition (Figure 19). Our tentative explanation based on visual inspection of the Geostationary Satellite Server (GOES) images (not shown) is that these low clouds were formed over the river and advected to the T3 site. To complete the comparison of the radiative variables, we show in Figure B1 the evolution of the incoming shortwave (SWin) and PAR 10 September. IFS and observations show a better match before noon, whereas DALES overestimates it. Under the presence of clouds, the agreement becomes better for DALES and observations whereas IFS tends to underestimate probably to an increase in cloud thickness. Furthermore, this comparison confirms us that, as a first approximation, the parametrization of PAR as equal to 0.5·SWin describes satisfactorily the evolution of this variable.

After 12 LT, DALES closely matches the observational climatology of the diurnal cycle during the hours in which the shallow cumuli layer is thicker, and when the explicit coupling between radiation perturbation by clouds and forest responses may play a role in modulating the amount of radiation reaching the canopy top. The specific observations of 10 September also show fluctuationg Qn values higher values than the clear-sky values due to the contribution of cloud reflection. It is important to stress that DALES is able to reproduce these short-term fluctuations, but it is still missing the cloud-side reflection due to the use of a one-dimensional radiative transfer representation. With respect to IFS, Qn slightly underestimates the observed values around 11 LT due to the greater cloud thickness. This general observation-model agreement in the available radiation range confirms that the amount and timing of energy reaching the canopy top are very similar before and after noon, and the next question is therefore how this energy is partitioned between the canopy-top turbulent fluxes.

Closely related to the canopy-top momentum flux, the friction velocity above the canopy comparison between observations and DALES is shown in Figure 6. The underestimation of the DALES results by more than 0.1 m s^{-1} indicates the need to resolve explicitly the interaction between the canopy and the atmosphere above the canopy throughout the entire day. As shown explicitly by Patton et al. (2003) and parametrized by Harman (2012), turbulence in the roughness sublayer (roughly defined as two to three times the canopy height) is enhanced with a dense and high canopy such as the tropical forest. In both models, we represent

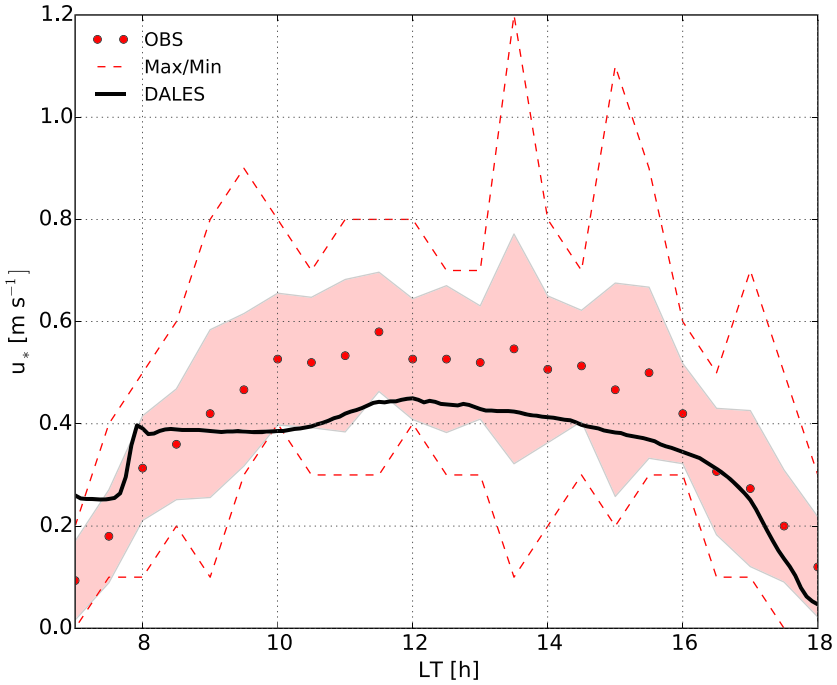

Figure 6. Observed and simulated friction velocity. Observations (mean, standard deviation, and maximum and minimum) refer to the entire month of September 2014 and were collected during the GoAmazon campaign. Observations were made above the canopy at the T0 Ksite.

the canopy layer as a bulk layer with more detail regarding the radiative transfer than the turbulent dynamics and heat/water/CO_2 exchange. For the former, we represent sunlit and shaded leaves, and we take the enhancement of diffuse radiation into account (Pedruzo-Bagazgoitia et al., 2017). However, in both models, the dynamic effects related to changes in the turbulent flow just above the canopy are only represented by high values of the roughness length. As found by Ouwersloot et al. (2016), the explicit simulation of the canopy effects on turbulence requires finer and isotropic grids ($1 \times 1 \times 1$ m^3). Less-demanding grid cell resolution, such as the anisotropy grids defined by $8 \times 8 \times 2$ m^3 resolution proposed by Gerken et al. (2017), is however still capable of capturing the main interactions between the within- and above-canopy flows. However, if we employ these demanding numerical resolutions to obtain better results for the friction velocity, the numerical experiments will be limited in terms of the sizes of the horizontal and vertical domains that are needed to study the full extent of the coupling between radiation perturbations by clouds, surface dynamic heterogeneity, and the turbulent transport of the state variables, which are key aspects of our goals. Therefore, we chose to prescribe a coarse resolution at the canopy layer in order to benefit from the explicitly solved interaction between clouds and vegetation. Section 6.3 discusses in more detail the impact of the coarse numerical resolution on the CO_2-tower measurements.

Before we present the comparison of the canopy top energy turbulent fluxes, it is necessary to discuss the nonclosure in the observed surface energy fluxes. In general, we expect that the observations of the canopy top turbulent fluxes for heat and moisture will be lower due to the lack of contributions of the lower frequencies of the turbulent fluxes driven by formation of secondary atmospheric circulations (Foken, 2008). Though this imbalance can be corrected by distributing it proportionally, by preserving the Bowen ratio, over the sensible and latent heat fluxes (Twine et al., 2000), we decided here to show the observations without including this correction.

The diurnal evolution of the sensible and latent heat fluxes is shown in Figures 7 and 8. Starting our analysis with the DALES results and the observations, SH is approximately 30% larger than the monthly-aggregated observations from the morning hours, although the agreement improves in the afternoon. Similarly, on 10 September, DALES overestimates the observed morning values. As discussed above, SH observations measured using the eddy-covariance technique are normally lower than expected, and it is therefore convenient to relate the diurnal evolution of SH to other variables such as the evolution of the cloud base

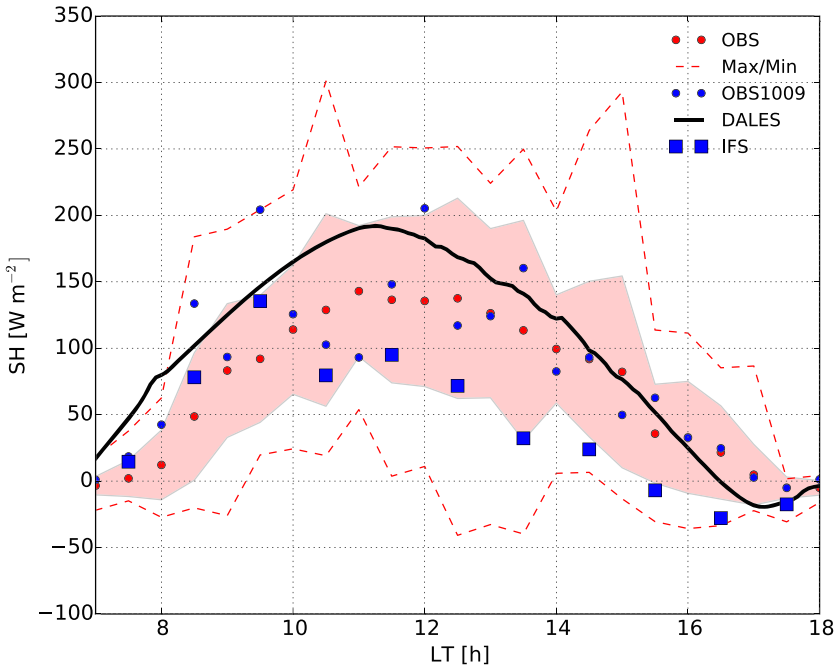

Figure 7. Same as Figure 5 but for the sensible heat flux.

(see Figure 18b) to determine how reliable they are in representing SH. Here, we take the cloud base as a proxy for the boundary-layer depth that is directly related to the magnitude of SH. The satisfactory agreement between DALES and cloud-base observations tells us that the SH calculated by DALES, and in the absence of large-scale forcing such as subsidence, is the main driver of boundary-layer dynamics, in addition to the entrainment process controlled by the upper atmospheric conditions, during the clear to cloudy transition. Regarding LE, the general diurnal pattern compares well with the observations until 12 LT, with an overestimate in the afternoon that is probably related to the partial closure of the rainforest CO_2 assimilation after midday (see discussion in section 5). Note that in both models, the water and carbon cycle are intrinsically linked through the stomatal aperture responses, represented in the A-gs model by the canopy surface resistance (Ronda et al., 2001).

Turning our attention to the IFS results, the morning value (9.30 LT) of SH is closer to the monthly-average observation compared with DALES, and the IFS LE results compare well with both observations and DALES. After midday, the IFS-LE representation calculates slightly higher values, negatively correlated with the lower values of SH (Figure 7). Here we have two plausible explanations: (i) For SH, the increase in the thickness of the shallow cumuli leads to a large decrease in the afternoon values; (ii) for LE, the higher CO_2 assimilation rates (as will be discussed in section 5) yield larger values of transpiration.

We relate our findings to the results obtained by Gerken et al. (2018). Working at the same T0k location as our simulated domain and during the same period of the GoAmazon2014/15 campaign, they reported that values of the residual of the surface energy balance oscillate between 80 and 100 W m^{-2}. Their analysis is relevant to our study, on the basis of the information flow analysis (Shannon entropy), regarding which flux in the surface energy balance provides information on the imbalance. Gerken's results demonstrated the dominance of evapotranspiration and radiation in determining the imbalance during the forenoon development of the boundary layer, and its relation to changes in energy storage and cloud cover. These results indicate the need to study and represent simultaneously the coupling between cloud radiation perturbations and canopy-top fluxes. At the Cuieiras site, whose rain-forest characteristics are similar to our site, dos Santos Michiles et al. (2008) obtained similar values to ours regarding the quantification of the nonclosure of the surface energy balance, up to 18%. The study discussed the relevance of energy storage within the canopy, in particular storage in the atmosphere and in tree trunks during the dry season (the total may reach maximum values of 60 W m^{-2}). Our results are also in agreement with the findings of Machado (2000), which quantitatively demonstrated that under clear-sky conditions, the surface exports less energy than it gains.

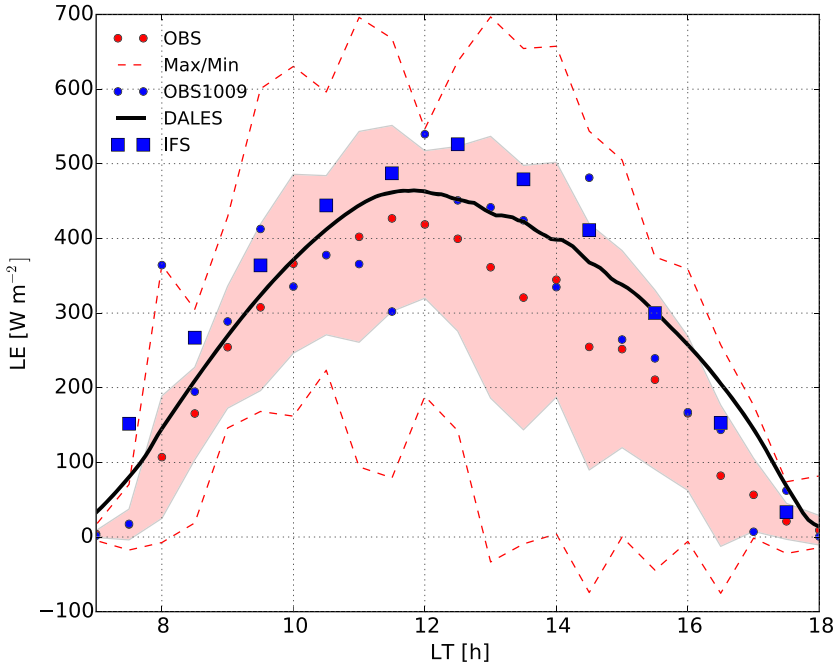

Figure 8. Same as Figure 5 but for the latent heat flux.

Placing these results in the perspective of the canopy-top turbulent fluxes, a finer resolution near the interface between the forest canopy and overlying atmosphere could enhance the turbulent mixing, as well as improving calculations of gradients and fluxes and the more advective fluxes dominated by ejections and sweeping motions at the canopy-atmosphere interface (Finnigan et al., 2009). Relevant to our analysis, and as we discuss in the following section, is the capability of the mechanistic representation of CO_2 plant assimilation to reproduce the CO_2 fluxes above the canopy.

5. Fluxes of Carbon Dioxide

By analyzing the plant, soil, and net fluxes of carbon dioxide (the generic flux is represented by FCO_2) above the canopy (Figure 9), we found that, before 10 LT, both models reproduce well the magnitude of the NEE observed with a tendency by IFS to underestimate after 10 LT; that is, more CO_2 is remove from the atmosphere. We partly attribute the better agreement between DALES and the observations to the coupling between radiation perturbations, surface turbulence responses, and the subsequent transport of heat and clouds as shown in by Figure 1. Pedruzo-Bagazgoitia et al. (2019) compares explicit large-eddy simulation experiments to parametrized mesoscale ones, both solving the interaction between shallow cumuli and vegetation. They showed that the explicit solution of the cloud-plant coupling among processes yield more realistic results regarding the shallow cumuli diurnal cycling and its impact on surface processes. The NEE observations show that the active CO_2 sink stops at around midday. This indicates a down-regulation of the plant assimilation activity that is driven by a combination of factors, including a reduction in PAR by clouds, and the more dominant effect of higher values of atmospheric water vapor pressure deficit in the afternoon, that is, midday depression (Doughty et al., 2006; Lin et al., 2019). By connecting these findings with the two regimes defined by the net available radiation (before and after cloud formation at approximately 10.5 LT), we could potentially establish a relationship between the onset of shallow cumuli and the reduction in plant assimilation activity that shifts the canopy-top energy balance toward higher values of the sensible heat flux (Vilà-Guerau de Arellano et al., 2012; Gentine et al., 2013). In turn, the rise in SH can be offset by a fall in the incoming shortwave radiation due to the greater cloud cover. Regarding the performance of both models, DALES results indicate that NEE becomes a source after 14 LT, whereas for IFS, CO_2 uptake remains the dominant process until 16 LT, that is, GPP > absolute(RES), where GPP is the gross primary production and RES is the soil heterotrophic respiration, respectively. Although it decreases slightly in the afternoon, the GPP flux in the IFS model remains quite high and in combination with the respiration leads

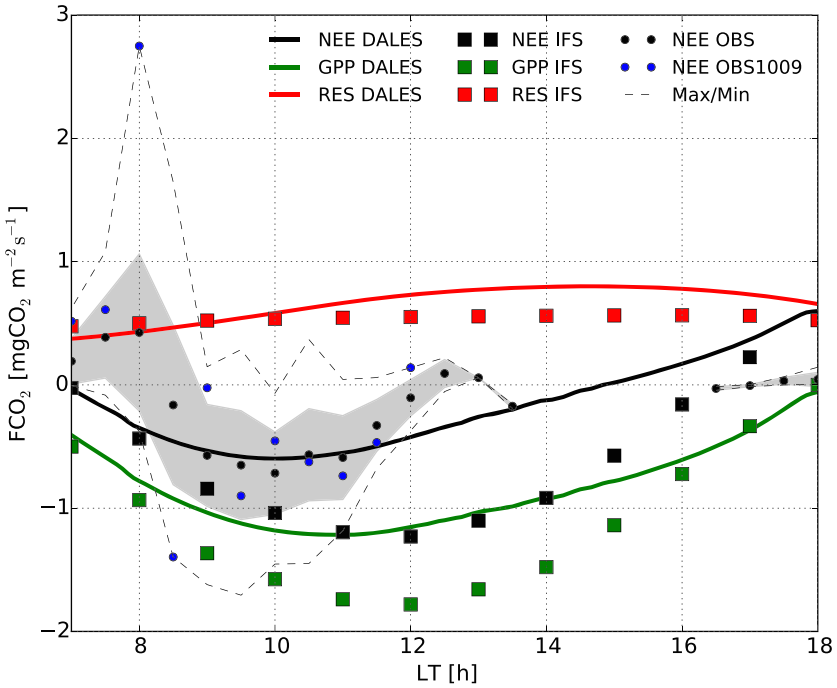

Figure 9. Evolution of the observed and modelled (DALES and IFS) net ecosystem exchange (NEE). The IFS and DALES model results of the canopy assimilation (GPP) and soil respiration (RES) are also included. NEE observations (mean, standard deviation, and maximum and minimum values) refer to the entire month of September 2014 and were acquired during the GoAmazon campaign. Observations were made above the canopy at the T0k site. Observations are missing between 14 and 16 LT.

to a late switching between the sink and source CO_2 regime. This could be also attributed to the simplistic parametrization of the ecosystem respiration. In other words, the modeling of the partitioning of NEE between GPP and RES is still uncertain and difficult to simulate during the afternoon transition when PAR is affected by clouds and water vapor pressure deficit (WVPD) is increasing.

Malhi et al. (1998) and von Randow et al. (2004) observed similar values of NEE during the dry season. During the period of maximum assimilation activity, from 10 to 12 LT, they showed minimum absolute values ranging from −0.7 to -0.6 mg m^{-2} s^{-1}. Relevant to our study is their finding related to the asymmetry in assimilation between the morning and afternoon periods. von Randow et al. (2004) discussed the different uptake rates in the afternoon. They explained it in terms of an increase of WVPD, defined as the difference between the saturated vapor pressure at the air temperature and the water vapor pressure at the same starting time and place. The WVPD, as well as the plant hydraulics, controls stomatal aperture and thus the exchange of CO_2 and H_2O at canopy level. In tropical forest, WVPD is the dominant control variable, which reduces the assimilation rates under high light levels (Fu et al., 2018). Both DALES and IFS include this dependence in their mechanistic model of plant physiology. It is represented by means of a parametrization that relates the gradient between the internal leaf CO_2 concentration and the atmospheric concentration as a function of the WVPD (Ronda et al., 2001). However, Figure 9 shows that the GPP calculated by IFS has a longer diurnal amplitude and more negative values than DALES, which might be a reason for the longer period with negative NEE values calculated by IFS. The switch from a CO_2 sink to a CO_2 source can be very sensitive to this CO_2-assimilation representation, and its link to variables depending on clouds, such as radiation, and on boundary-layer evolution like entrainment. It also depends on the soil respiration, which is a function of soil and in-canopy properties. With respect to the CO_2 respiration efflux, DALES and IFS agree satisfactorily. As Figure 9 shows, there is a slight rise in the DALES model results due to higher soil temperature, probably related to the nonexplicit representation of in-canopy processes (see discussion of Figure 5). Connecting our findings with observations of the soil respiration in the same region, DoffSota et al. (2004) reported average values of 0.28 mg m^{-2} s^{-1} and maximum values of 0.43 mg m^{-2} s^{-1}, which indicates that both models slightly overestimate this respiration flux compared with characteristic values observed in the Amazonian rainforest during the dry season. Similar values were reported by von Randow et al. (2004).

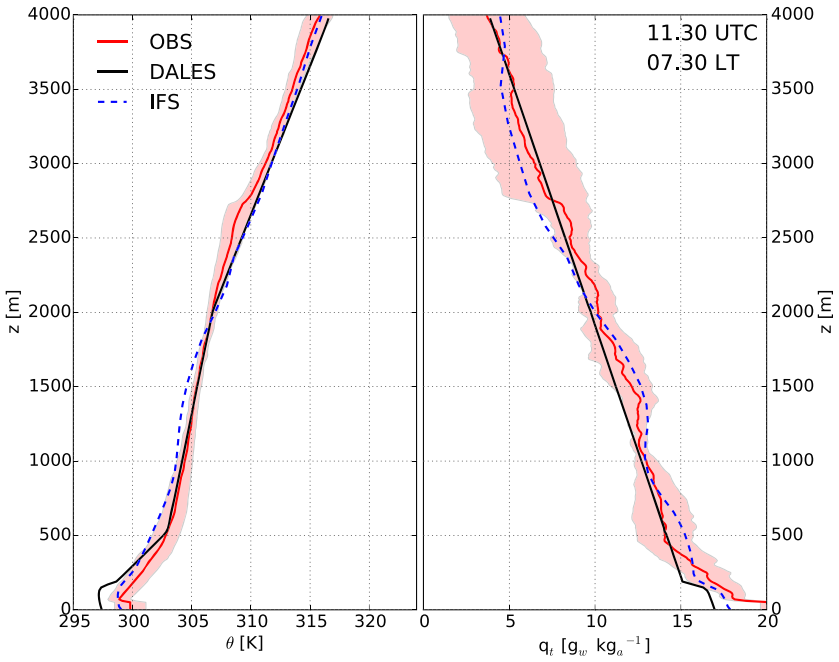

Figure 10. Observed and simulated vertical profiles of the potential temperature and specific humidity. The figure shows the mean and standard deviation of the sounding observations launched around 11.30 UTC. Soundings were launched at the T3 site.

6. Thermodynamic Vertical and Carbon Dioxide Structure

6.1. Before and Onset Shallow Cumuli Formation

The profiles of potential temperature (θ) and specific humidity (q) at 07.30 LT (1.5 hr after DALES initialization) are shown in Figure 10. The layer characterized by well-mixed conditions just above the canopy (≈135 m) marks the difference in agreement between the model and the observations. The DALES profiles above this height closely follow the averaged monthly observations due to the initial profiles imposed, which were constrained by the radiosoundings (Table A2). Due to the similarity in thermodynamic characteristic with the Atlantic Ocean shallow cumuli (Siebesma et al., 2003), this provides a first indication that the upper-atmospheric thermodynamic state profiles are largely determined by the advected air masses that originated from the western Atlantic Ocean and further influenced by the 1,500 km of travel over land (Burleyson et al., 2016). Furthermore, as inferred by the surface heterogeneity, in our specific case rivers, secondary circulations might arise that can influence these thermodynamic vertical profiles. This can be seen, for instance, in the absence of clouds above the rivers as shown in Figure 2. Below 135 m, DALES and IFS model a colder and drier mixed layer compared to the observations. This disagreement might indicate the influence of the tall forest canopy on the local surface turbulent fluxes, which are crudely represented by DALES and IFS.

Garstang and Fitzjarrald (1999), based on the observations collected by Martin et al. (1988), defined five stages in the evolution of the boundary layer in tropical forest regions. Our model results reproduce the transition between the first and second stage that corresponds to the rapid formation of the convection-driven boundary layer and the subsequent engulfing of the residual layer. The latter is largely determined by the advected air masses and the previous day's disturbance caused by the presence of shallow and potential deep convection. An efficient transport of moisture combined with an enhancement of thermal instability at the height of the shallow cumuli cloud base could create better conditions for the development of the deep convective state (Wright et al., 2017). Above the canopy, and as found by Anber et al. (2015), and during the morning transition, the potential effects of low stratified clouds during the morning transition are not reproduced by DALES. Future numerical experiments that specifically address the role of the morning low clouds will require initialization during previous evening, finer vertical resolution, and more detailed representation of microphysics and canopy.

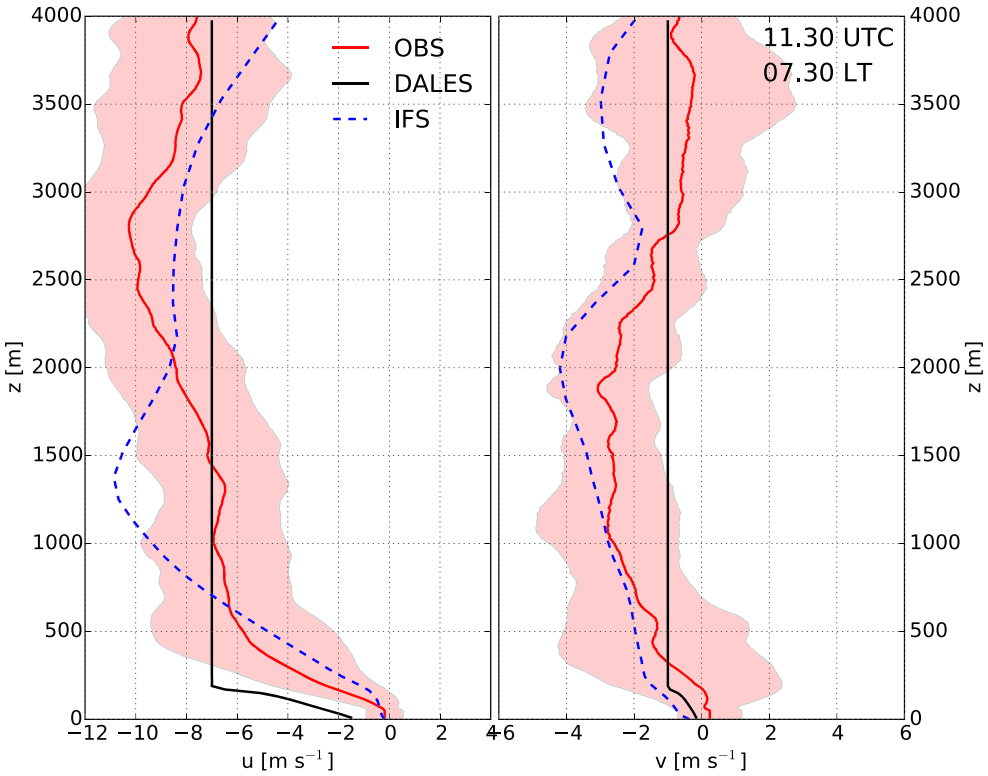

Figure 11. Same as Figure 10 but for the two velocity components u and v.

Figure 11 presents the profiles for the two wind components u (west-east direction) and v (north-south direction) at the same time. DALES- and IFS-calculated wind profiles follow the observations with their monthly variability. Compared to IFS and the observations, DALES wind variability after 1.5 hr of the simulation is only noticeable below 135 min the well-mixed layer, and the profiles above are still influenced by the initial conditions imposed. They therefore miss the presence of local shear turbulent production as observed and reproduced by IFS at altitudes above 135 m.

Figures 12 and 13, simulation at 14.30 UTC, show a more intense and deeper turbulent layer for both IFS and DALES. In other words, both models require long integration period to spin up of the turbulence. The physical explanations behind are different. For DALES, we begin with a laminar layer that requires at least more than 1 hr, partly due to lower values of SH, to become turbulent due to the lower values of the buoyancy. For IFS, the transition between the stable and unstable turbulent regimes becomes faster than DALES. As shown by Figure 12, the well-mixed layer develops at 14.30 UTC (10.30 LT) are 300 m deeper than in DALES. Regarding the u and v wind components, DALES profiles are characterized by better well-mixed conditions than IFS, which could indicate that the turbulent mixing in the IFS is more efficient for heat and moisture compared to momentum. IFS and observations show the dominance of the east to west direction in the entire low troposphere that corroborates the maritime origin of the air masses over this region.

6.2. Mature Shallow Cumuli Convection

Figures 14 and 15 show the evolved thermodynamic profiles at 17.30 UTC. To complete the discussion and avoid the loss of information due to the averaging of multiple radiosoundings, we add the observations of a profile gathered on 15 September (OBS1509), in absence of radiosoundings for 10 September. This day (15 September) was also characterized by only shallow convection, and absence of deep convection development. At 13.30 LT, shallow cumuli are fully developed with cloud cover close to 30% (see Figure 19). DALES-calculated profiles reproduce the observed $\theta-$ and $q-$ vertical variation. They are characterized by a well-mixed subcloud layer up to 1,200 m, which is connected to a cloud layer that reaches 4,000 m. IFS reproduces these two layers well, but there is a large difference at the interface between the subcloud and cloud layers. At this interface, IFS shows larger discontinuous jumps in the potential temperature and specific humidity. For the latter, we find a difference of almost 3 g kg^{-1} between the IFS results and the observed

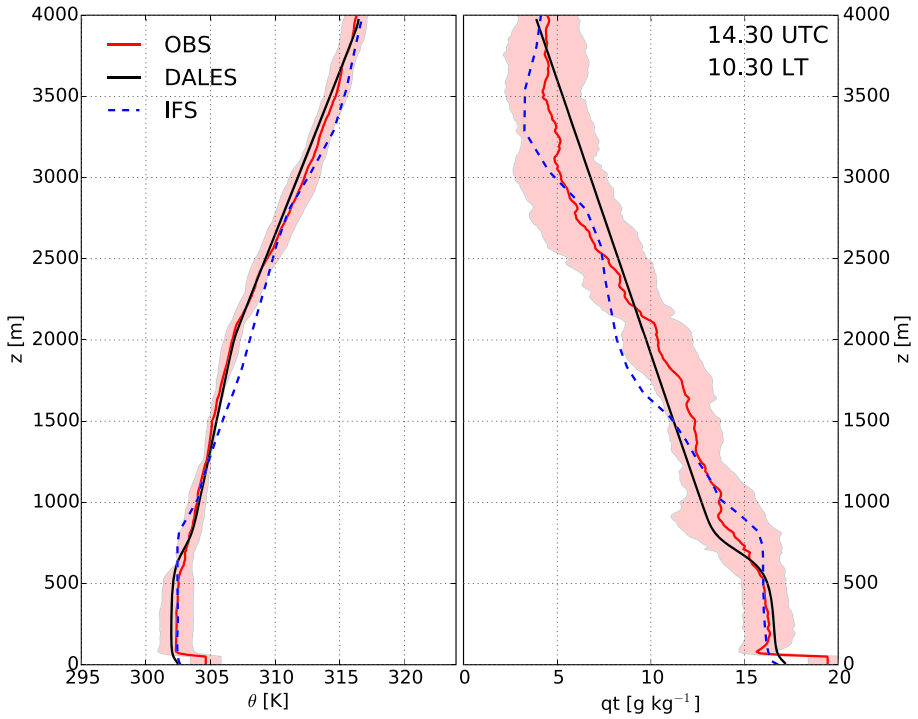

Figure 12. Same as 10 but around 14.30 UTC.

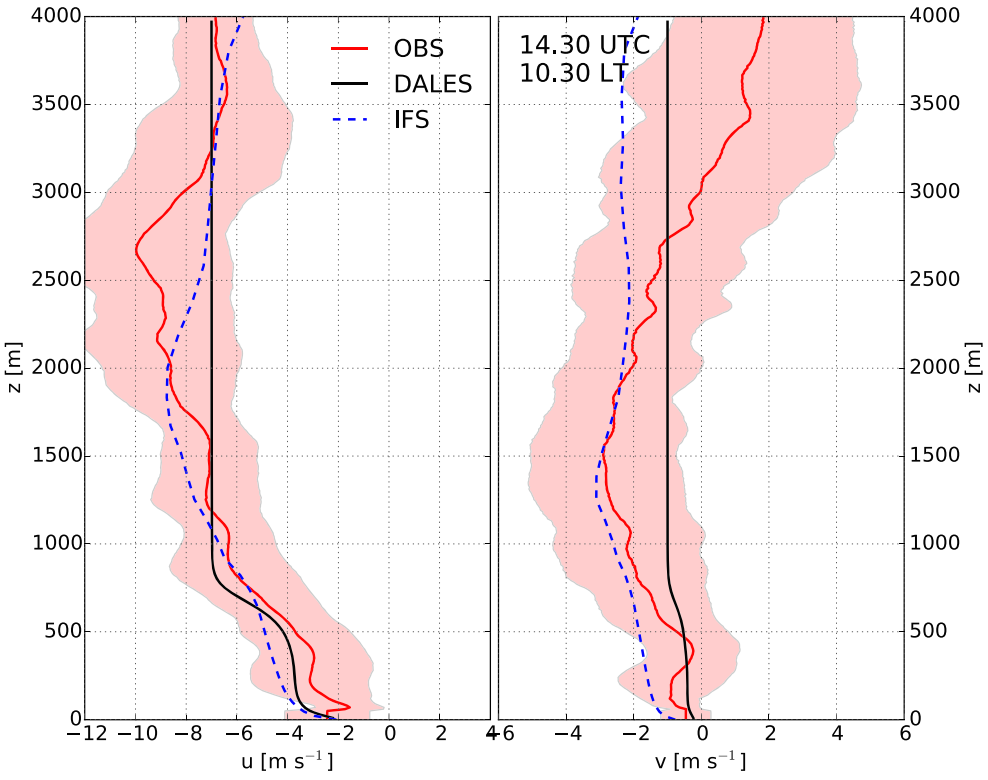

Figure 13. Same as Figure 11 but around 14.30 UTC.

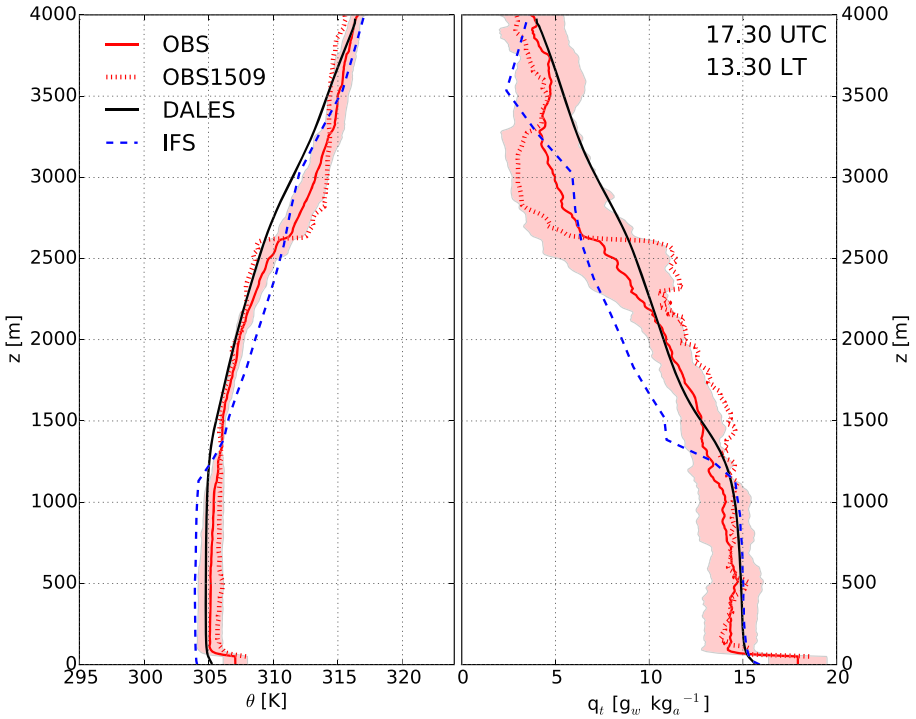

Figure 14. Same as 10 but around 17.30 UTC. The θ and q profiles (OBS1509) measured by a radiosounding launched at 17.28 UTC on 15 September 2015. This day was characterized by similar shallow cumulus conditions as 10 September.

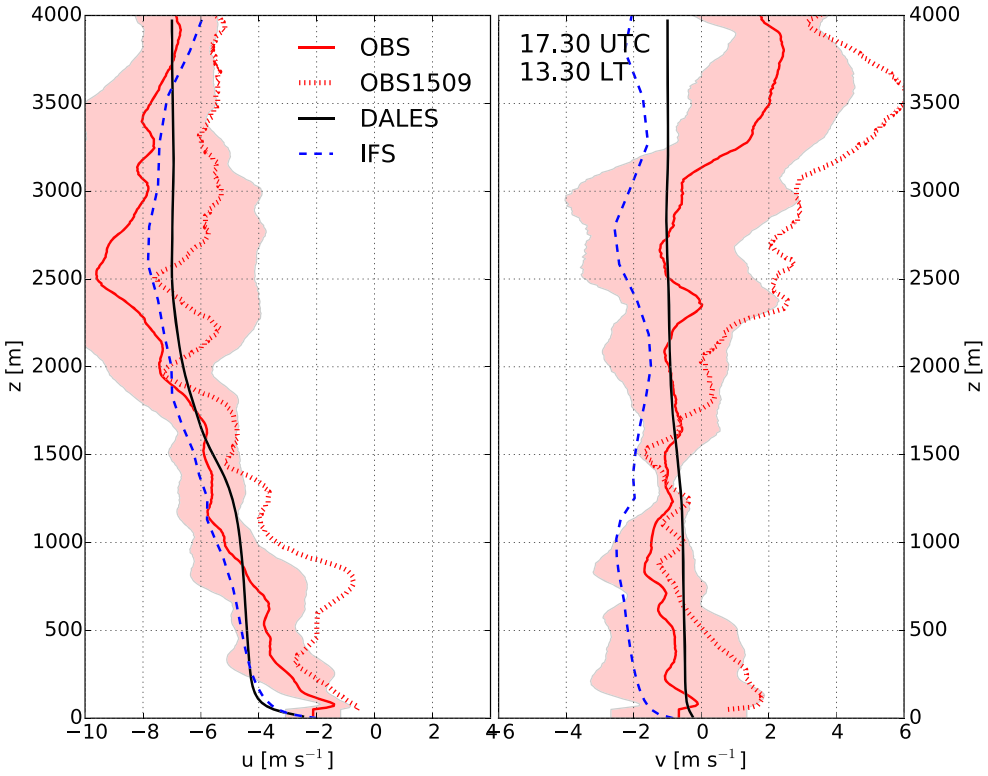

Figure 15. Same as Figure 14 but for the two velocity components u and v.

and DALES results. Although sharper features are found in the OBS1509 data, the θ- and q-measured profiles are in close agreement with DALES and the observed-aggregated profiles. Focusing on the IFS results, we explain the the formation of $\theta-$ and $q-$ gradients at the interface between the subcloud and cloud layers due to inefficient turbulent mixing and the shallow convective mass flux parametrizations.

The inefficiency of the the moistening transport could have a direct impact on the triggering of deep convection, since thermal instability can be a limiting factor. Based on the IFS results, Zhuang et al. (2017) showed in their Figure 2 a reduction of around 100% of the calculated monthly precipitation during the month of September (average years 2014 and 2015) due to the coarse vertical resolution. The misrepresentation of moist entropy in the lower troposphere controlled by the coupling radiation-surface-turbulence could lead to a weakening of the shallow convection moisture pump, and the subsequent delay of the onset of the wet deep convective season (Wright et al., 2017). Finally, and analyzing OBS1509, we found a key feature in the θ and q profiles at 2,600 m, that is, is the presence of a strong and sharp inversion characterized by an increase of 4 K and a decrease of 7 g kg^{-1}. As such, this inversion is an additional factor that might prevent the transition to deep convection, and to reproduce it with DALES will require imposing different initial profiles and including more complex microphysical processes.

With respect to the two wind components u and v, which at this period display peak activity, the agreement between the measurements and the DALES and IFS profiles is within the range of the observational variability. In particular, and focusing on the more dominant u component, both models reproduce well the magnitude of shear that is characteristic of the subcloud layer and the lower part of the cloud layer. However, the zonal wind (u) in the first 500 m is overestimated, which could be related to a canopy effects in the first 100 m and enhanced transport of momentum in the lower atmospheric boundary layer. These disagreements below 500 m are further widened by the u and v profiles of 15 September that show a larger shear in magnitude and direction. Our explanation here is that the combination of canopy effects (roughness sublayer relevant in the first 150 m) and mesoscale effects triggered by topography and the presence of rivers can play an important role in the wind profiles above the canopy top.

To complete the profiling intercomparison, Figures C1 and C2 show the θ, q, and two wind components profiles at the end of the evening transition. The establishment of stable stratified nocturnal boundary layer with a height of 250 m is evident from the observations and IFS. IFS is able to represent this because of the activation of the parametrization of the stable boundary layer. However, DALES would require a higher vertical resolution (for instance 5 m or lower values instead of the 20 m used) to represent explicitly the smaller eddies characteristic of the stable stratified conditions and therefore to capture the collapse of turbulence during the evening transition.

6.3. CO_2 Mixing Ratio: Evolution Above Canopy and Profiles

With regard to the diurnal evolution of the CO_2-mixing ratio presented in Figure 16, we find that both DALES and IFS reproduce well the observed diurnal minimum evolution but the diurnal CO_2 variation, that is, the difference between maximum and minimum diurnal values, is larger for IFS. Between observations and IFS-DALES and during the period between 10 and 16 LT, the maximum differences occur during the morning transition and diminish during the afternoon (maximum 3 ppm). We explain this disagreement by a combination of factors. First, the morning transition from stable to unstable conditions at the interface canopy-atmosphere still presents a challenge for both models. Particularly for IFS, the combination of steep thermal gradients and the accumulation of CO_2 in the canopy as a result of the CO_2 ecosystem respiration leads to very large values in the layers above the surface. This can be seen by the significant overestimate of the IFS results at 10 LT (more than 5 ppm). In the case of DALES, we prescribed initial conditions in accordance with the early morning observations, and the agreement is better. Second, the CO_2 minimum value is controlled by two processes: NEE (the net flux between plant uptake and soil respiration) and entrainment. As Figure 9 shows, both models simulate a longer period characterized by negative NEE (sink), but for DALES the CO_2 plant uptake is not strong enough. The minimum level of CO_2 is also largely controlled by the entrained air from the residual layer (Vilà-Guerau de Arellano et al., 2004) and is therefore dependent on the mixing ratio values in the residual layer. The lack of phase between the diurnal variability of NEE and the entrainment of low CO_2 air from the nocturnal residual layer is therefore crucial to obtain CO_2 model results that become closer to the observed CO_2 minimum diurnal values.

The discrepancy between observations and modeling is further accentuated by the crude description, in both models, of the role played by the canopy in governing the interaction of thermal stratification and induced

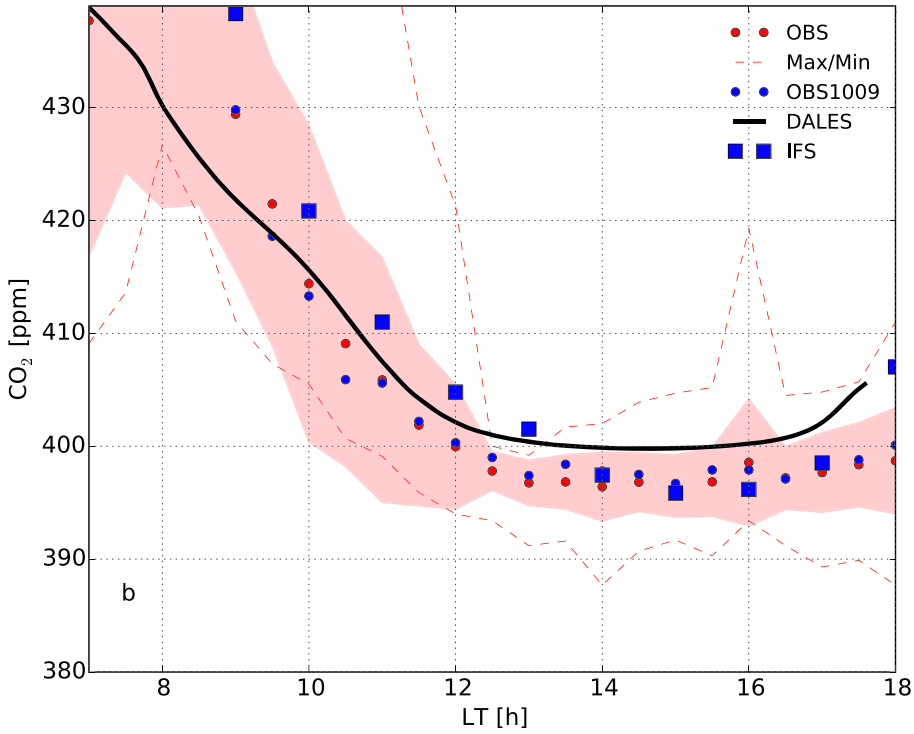

Figure 16. Temporal evolution of carbon dioxide mixing ratio calculated using DALES and IFS. Observations were made at 48.2 m at the T0 K site. The observations are a composite of the monthly averages.

canopy turbulence. As shown in the inset of Figure 17, the differences between the CO_2 mixing ratio above the canopy can be very large in both models, and particularly in the IFS model. It is worth mentioning that the evolution of the CO_2 mixing ratio is due to the contributions of several processes: the local NEE CO_2 soil and canopy processes and the combined nonlocal effects of entrainment and horizontal advection. For the former, DALES reproduced well the net CO_2 sink (Figure 9), but in spite of this, CO_2 is still overestimated. Therefore, it is instructive to analyse the evolution of the CO_2 profiles.

Figure 17 shows the CO_2 profiles in the early morning (7.30 LT) and early afternoon (13.30 LT). At both times, the inset figures show the profiles in the lowest 60 m compared with the available observations. Note that the canopy height ranges between 30 and 35 m. In the first 1,500 m, we find clear differences between the DALES and IFS model results, and observed profiles. Values in the cloud layer are very similar, since the initial CO_2 profile imposed in DALES was prescribed as a combination of canopy-top observations before dawn and the IFS profiles in the free troposphere. Above the canopy top, steeper CO_2 gradients are calculated by IFS in the atmospheric boundary layer. They are the result of the accumulation of CO_2 at the model level closer to the surface, due to the combination of the stable stratified layers and the CO_2 ecosystem respiration during the night. In the course of the day, the CO_2 plant assimilation sink becomes more active and leads in turn to lower concentrations compared to DALES and the observations. It is relevant to stress that unlike the well-mixed θ and q profiles, the IFS results show a CO_2 gradient in the subcloud layer, which we attribute to the overestimation of GPP during the day. Under convective conditions similar to the those under analysis here, and provided that the net ecosystem exchange and the entrainment of carbon dioxide is adequately represented, well-mixed profiles of CO_2 have been observed (Vilà-Guerau de Arellano et al., 2004).

With respect to the heights near the surface (first 60 m), either models is able to reproduce the observations located just above the canopy top at 53.1 m: There is an overestimate by DALES, while the IFS results move from an overestimate to an underestimate. As Figure 16 shows, DALES results keep this overestimation during the entire day whereas IFS values reproduce a a larger CO_2 decrease over time, with a satisfactory agreement with the observations in the afternoon (from 14 to 17 LT). Our conclusion here is that just above the canopy, both models are capable of reproducing the main diurnal trend but it will be necessary to further validate the CO_2 vertical profile at the interface. Near the canopy top, the CO_2 mixing ratio below 60 m

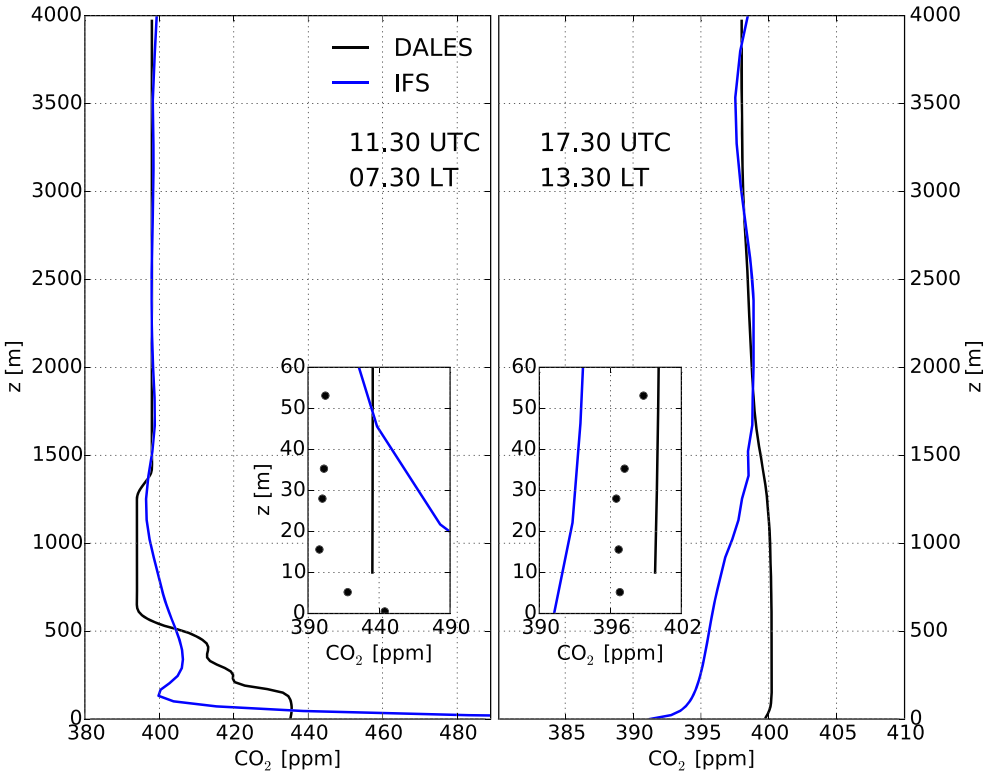

Figure 17. Vertical profiles of carbon dioxide calculated by DALES and IFS. The inset shows the comparison of the observations in and above the canopy and the the DALES and IFS results of the three levels just above the canopy top.

is still misrepresented, due to the combination of local forest-turbulence effects, the nonlocal contributions of entrainment, and the large-scale effects driven by the transport of air masses.

7. Evolution of the Cloud Main Characteristics

Figure 18 shows the evolution of the cloud top and base and the boundary layer height (z_i) modeled by DALES and IFS. When comparing these results with the observations, note that the observations also include days in September on which deep convection was active and our DALES results are only representative of the shallow convective phase (approximately until 15 LT). As a result, this degree of variability is a direct consequence of the aggregated approach, where an offset in timing and intensification leads to a wide spread of values. We therefore focus on the ability of the model to reproduce the transition from clear to shallow cloud conditions, and the main characteristics once the shallow cumuli are mature. As modeled by DALES and IFS, the boundary layer clouds until 11 LT are forced and display small vertical development. From 7 to 11 LT, the boundary-layer height, defined as the altitude where the minimum value of the buoyancy flux, rises steadily from 100 to 1,000 m. It is at that time that the cloud top rapidly rises, reaching around 4,000 m at about 13 LT. The hourly observations from 12 to 15 LT show values that range from 3,200 to 4,700 m. The DALES observations are in close agreement with these cloud-top observations corroborated by the limited number of observations of the W-cloud radar, which they range from 3,368 m at 14 LT to 4,129 m at 18 LT, with a maximum value at 17 LT of 4,291 m. Note that the vertical extent of the clouds reaches the top of the DALES vertical domain, but the numerical experiment shows that shallow cumuli do not spread horizontally at the top due to this limiting vertical domain. This is further corroborated by the values of the buoyancy flux, which are close to zero at the domain top (Figure D1b).

After 15 LT, the monthly mean observations show a deepening of the clouds, indicating that on certain days in the dry season, there is a transition to deep convection. Regarding cloud base height, DALES and the observations are in close agreement, reaching a maximum height at 16 LT. IFS results follow the observations satisfactorily until 11 LT, but 3 hr later they underestimate the cloud base height by 300 m. Regarding IFS, note that throughout the entire cumulus period, z_i and cloud base share the same value. We attribute

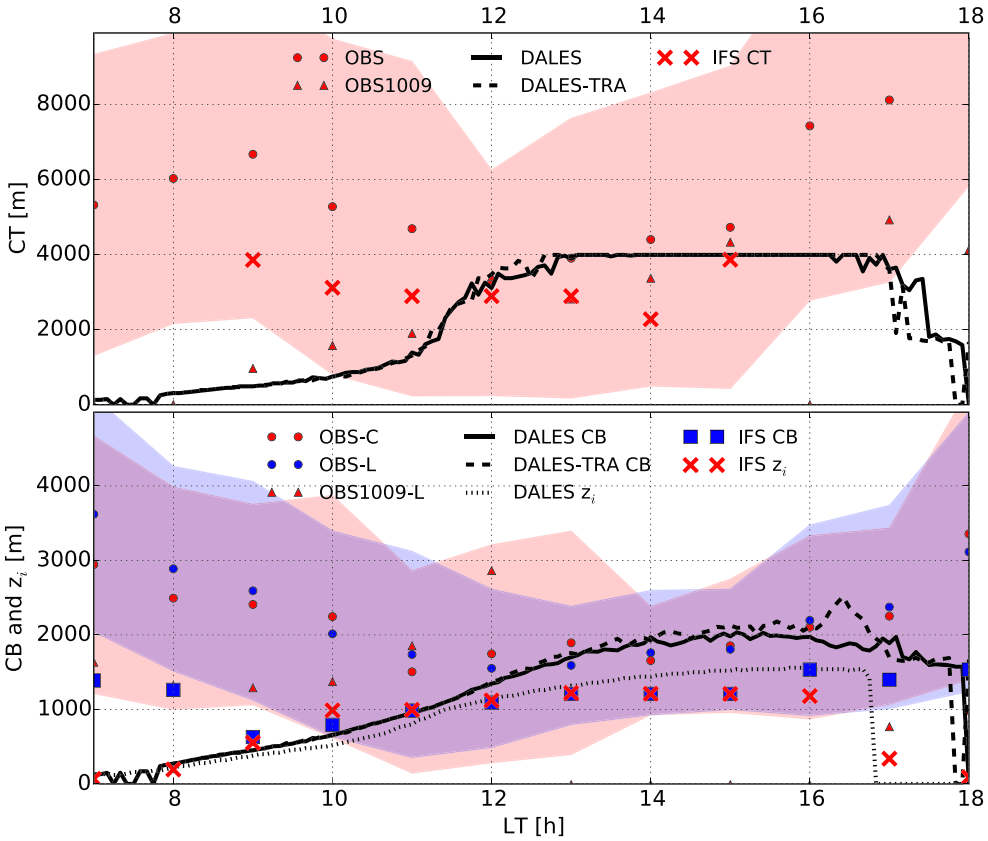

Figure 18. Simulated evolution of the cloud top height (upper panel) and cloud base and boundary-layer height (z_i) (lower panel). Observations from the cloud top were retrieved from the cloud radar (W band). Observations of the cloud base were inferred from the lidar (L) and ceilometer (C) readings. All the observations were gathered at the T3 site. The shaded region indicates the standard deviation of the measurements. DALES initial and boundary conditions are prescribed to start with a clear atmospheric boundary layer. DALES-TRA shows the results with transparent radiative clouds.

this underestimation to the relatively inefficient transport of heat and moisture by the IFS mass flux representation, as is indicated by the formation of the potential temperature and specific humidity jumps as discussed in Figure 14. It is interesting to note the agreement between DALES and IFS regarding the collapse of the boundary layer at around 17 LT, and the subsequent formation of a shallow boundary layer. This is further corroborated by the low values measured by the LIDAR (OBS1009-L) at 17 and 18 LT: 768 m and 985 m, respectively.

The evolution of cloud cover and liquid water evolutions is in Figure 19. Focusing on the period 10 to 17 LT, the DALES results closely follow the observed evolution from cloudless conditions to maximum cloud cover of 0.3. After 14 LT, the DALES cloud cover begins to diminish, closely in line with the decline in the canopy-top turbulent fluxes. The observations show almost constant values between 0.3 and 0.4 until 16 LT when DALES shows that shallow cumuli are dissipating (18%) whereas the cloud cover by IFS is below 10%. Note that the observations refer to the monthly September average. There is thus a possibility that the shallow cumuli will further develop into deep convection. The IFS underestimates the low clouds (~10%). However, the medium cloud cover remains closer to the observations and DALES results until 13 LT, but with a clear decrease afterward. Finally, and to complement our analysis, we perform an extra experiment with DALES, in which the clouds are radiatively transparent (experiment TRA) but still active dynamically (Horn et al., 2015). This experiment is performed in order to determine the role of coupling between clouds and vegetation. The results, shown by the dashed lines in Figures 18 and 19, indicate a slightly higher cloud top, and high cloud covers, which on average are 5% larger than in the control experiment. These results are similar to those found by Sikma and Vilà-Guerau de Arellano (2019), who stressed their relevance to the amount of energy arriving at the surface and how it is distributed in space and time, in addition to the role

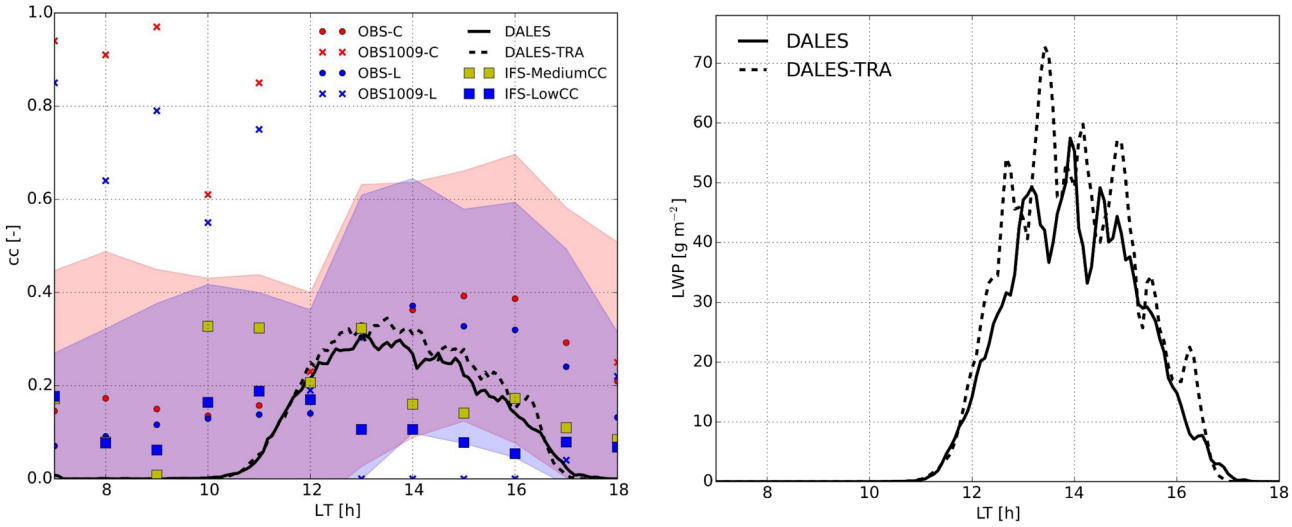

Figure 19. Simulated evolution of the cloud cover (left panel) and liquid water path (right panel). The IFS results show the low and medium cloud cover. Low clouds are defined as those that occur on model levels and with a pressure that lies between the surface pressure and 0.8 times the surface pressure, and medium clouds between 0.8 and 0.45 times the surface pressure. In our specific experiment low clouds are approximately between 0 and 2 km in height and medium between 2 and 6 km in height. Observations of cloud cover were retrieved from the lidar and ceilometer (C). The shaded area indicates the standard deviation of the observations. DALES-TRA shows the results with transparent radiative clouds.

of vegetation, by regulating the partition of the canopy-turbulent fluxes, in controlling key properties of the shallow cumuli dynamics, such as cloud cover and midtropospheric moisture convection.

Regarding the evolution of the liquid water path (LWP), Figure 19 (right) shows only the DALES results that correspond to the control and TRA experiments. The greater values of LWP corroborate the more vigorous clouds in the TRA experiment: For the control experiment the average value is 12.9 g m^{-2} and for TRA 15.8 g m^{-2}. As discussed by Cecchini et al. (2017), measuring liquid water content associated with smaller droplets (<50 μm), typically from shallow cumuli, remains a challenge. Comparing the above results with previous studies of shallow cumuli over land, we find that the evolution and LWP are similar. Over midlatitude areas characterized by lower moisture content, Lenderink et al. (2004) showed maximum values of LWP of 40 g m^{-2}. Measurements made by the microwave radiometer retrievals reported by Zhang and Klein (2013) at the Southern Great Plains Atmospheric Radiation Observatory indicate that values higher than 30 g m^{-2} are associated with clouds that exhibit deeper vertical development, that is, thick clouds.

The large vertical extent and intensity of this Amazonian phenomenon is further quantified by the fluxes of the liquid water potential temperature (Figure D1a), buoyancy (Figure D1b), total moisture, and liquid water (Figure D1c). All the fluxes exhibit strong diurnal variability and an efficient energy transport by turbulence originating in the canopy top and by latent heat release in the cloud layer (see for instance the higher values of the buoyancy up to 3,500 m) and liquid water flux. The buoyancy flux and the total moisture flux can be divided into two regions. In the subcloud layer (at 12 and 14 LT located at 1,244 and 1,593 m, respectively), they follow the characteristic flux profiles of the canonical convective boundary layer. In the cloud layer, the liquid water potential temperature and the total moisture flux decrease linearly, while the height of the buoyancy flux depends more on the intensity of shallow cumuli: a linear decrease in the early stages (12 LT) and almost constant with height during periods of maximum intensity (14 LT). In spite of the efficient transport by the clouds, the CO_2-flux profile (Figure D1d) shows that, on average, the mass flux transport of CO_2 is small, while the entrainment flux is, besides the assimilation of CO_2 by the rainforest, relevant during the period before the onset of shallow cumuli. Our explanation is that once the CO_2 from the residual layer is mixed into the atmospheric boundary layer during the morning, the CO_2 mixing ratio is relatively uniform. As a result, the impact of the mass flux driven by shallow cumuli on the vertical profile is highly dependent on the conditions of the atmospheric constituent of the subcloud and cloud layers. This effect requires more detailed studies using conditional averaging by selecting only buoyantly active clouds Ouwersloot et al. (2013) in order to better quantify the cloud venting.

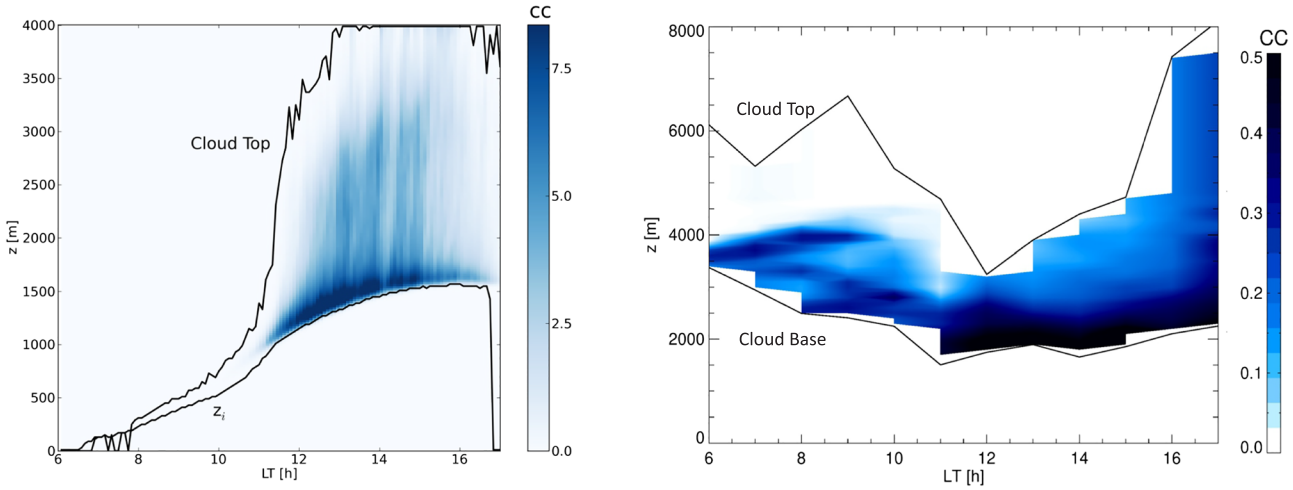

Figure 20. Left: DALES results of the cloud cover profile (multiplied by 100). The calculated boundary-layer height (z_i) and cloud top are indicated by the continuous lines. Right: aggregated observations of the cloud cover fraction (from 0 to 1) in September 2014. The cloud base and cloud top are shown by the continuous line. See the text for an explanation of the differences in the estimates of cloud cover.

To complete the comparison with the observations, the dependence of cloud cover on height is shown in Figure 20. Focusing on the hours from 11 to 15 LT, the ones more representative of shallow cumuli, we find that both DALES and observations indicate maximum cloud cover just above the cloud base. Maximum values of DALES averaged 15%, while the measurements are characterized by values of between 40% and 50%. This comparison is qualitative due to the different methods employed in calculating the cloud cover height dependence. DALES calculates at each time step, while the cloud cover measurement estimates were calculated by combining the lidar and W-band radar and were calculated as the percentage of the time (per 1 hr) during which any cloud was detected in a 100 m layer. Both observations and DALES show that during this period, clouds are limited in height (maximum values 4,000 m) and gradually rise after 12 LT. In DALES, the cloud cover decreases linearly with height, but this dependence is less clear in the observations. Note that the vertical extent of the clouds reaches the top of the DALES vertical domain, but the numerical experiment shows that anvils are not formed at the domain top.

8. Discussion and Conclusions

Motivated by the interaction between the Amazonian tropical forest and the dynamic spatial patterns formed by clouds, the *green-white ocean-atmosphere system*, we used our canopy-top and upper-atmospheric observations to evaluate systematically the numerical shallow cumuli experiments interactively coupled to vegetation. This study focuses on the final period of the dry season, in September 2014, which is crucial to the onset of the Amazonian tropical forest wet season. The models-observations comparison was performed by means of the turbulent-resolving large-eddy simulation DALES at high spatial (53 m × 53 m) and temporal (1 s) resolutions and the 9 km × 9 km resolution of the global weather model IFS. Both models represent photosynthesis and stomatal aperture with a similar mechanistic model that depends on photosynthetically active radiation, temperature, and water vapor deficit. The main difference between them is on the treatment of turbulence and cloud dynamics and their coupling with the surface responses: explicit for DALES and parametrized by IFS. As such, the DALES results simulated the bidirectional interaction between clouds and the tropical forest that are characterized by rapid (seconds) and spatially (meters) heterogeneous perturbations of the radiation and turbulence fields.

Our main findings are as follows:

- Radiative and surface turbulent fluxes above the canopy: The calculated radiative and canopy-top turbulent fluxes for momentum, heat, moisture, and carbon dioxide are all within the range of variability of the observed monthly September average. The comparison with observations is still uncertain due to the nonclosure of the measured surface energy balance and the presence of low clouds during the

morning transition. However, there is satisfactory agreement in the partitioning of the net available radiative energy into sensible and latent heat fluxes. Similarly, during the morning hours, the net contribution of CO_2-soil efflux (positive) and gross primary production (negative) is in satisfactory agreement with the NEE observation. In the afternoon, the NEE changes from a sink to a source 2 and 4 hr earlier in the observations than predicted by DALES and IFS, respectively. DALES performs slightly better than IFS in reproducing the transition from a negative to a positive NEE. Since both models employ the same vertical resolution, this could indicate that the explicit coupling between cloud and the forest with radiation, temperature, and water vapor pressure deficit could improve the calculation of photosynthesis and stomatal aperture, which are more sensitive to short spatiotemporal fluctuations.

- Mean meteorological and carbon dioxide levels and fluxes above the canopy:
  In both DALES and IFS, the diurnal variability of the state meteorological and carbon dioxide variables shows the correct order of magnitude and diurnal trend, but it indicates that at subdiurnal scales these variables depend on both the nonlocal processes (entrainment) and large-scale forcing, superimposed on local sources and sinks. When we relate these findings to the measurements made in and above the canopy, we find that within the roughness sublayer (between 30 and 60 m), the DALES and IFS results are both colder and drier than the observations. The CO_2-mixing ratio shows differences of around 3 ppm. These findings suggest that we need to explicitly represent the physical (radiation and turbulence) and within-canopy processes, associated with the need for high resolution to resolve the canopy-atmospheric dynamics.
- Vertical structure of the atmospheric boundary layer:
  The profiles of wind, potential temperature, specific humidity, and carbon dioxide agree with the observations. Both models reproduce satisfactorily the well-mixed profiles of θ and q in the subcloud layer and the unstable conditional conditions in the cloud layer. The shear in the entire cloudy boundary layer agrees well with the observations, since both models reproduce the variability on height of the wind speed. An important difference in this respect between DALES and IFS is that the latter calculates warmer and drier conditions at cloud base, which may influence the triggering of deep convection at later stages. As quantified by Wright et al. (2017), prior conditions to the onset of the wet season play a key role in setting more optimal conditions to enhance conditional instability. With respect to our study, a key condition is the upward mixing of moist air by shallow cumuli controlled by the surface turbulent fluxes and the heat release by phase changes above cloud base. In that respect, the explicitness calculation of turbulence at the interface between the subcloud and cloud layers provides a quantification that can improve future parametrizations of the mass flux and turbulent mixing.
- Temporal evolution of shallow cumuli:
  The transition from a clear to a shallow cumuli boundary layer (before 15 LT) quantified by the cloud base and top is well reproduced by both models. During the period of maxim intensity, we found that model and observations agree on a cloud base below 2,000 m and a vertical extension of the clouds that ranges between 2 and 2.5 km. This corresponds to cloud covers that range between 0.25 and 0.4 with maximum levels of cloud coverage. The DALES results are in agreement with the cloud cover observation in the early stages of shallow cumuli formation (until 14 LT) whereas IFS underestimates cloud cover (around 0.1 as an average value). The monthly composite observations show that there are days in the dry season that trigger the development of deep moist convection (after 14 LT). Although DALES results show that the cloud top may reach 4,000 m, the observations of the specific day and the level of buoyancy calculated by DALES indicate no further growth of the cloud layer, even though there is not an absolute thermal inversion.
- Coupling canopy and shallow cumuli:
  Based on an additional DALES experiment that imposed radiative transparent clouds, we conclude that the adequate distribution of the energy at the canopy top impacts relevant cloud characteristics such as cloud cover and liquid water path. In agreement with previous work (Sikma & Vilà-Guerau de Arellano, 2019), the absence of coupling leads to an intensification of the diurnal cycle of shallow cumuli. The inclusion of other processes such as more complex microphysics or three-dimensional radiation might play a role in invigorating the shallow convection, which suggests that the vertical domain of the numerical experiments will need to be extended to allow the vertical growth of clouds.

The numerical experiment settings and the comprehensiveness of the observational data set offer the possibility of extending this study to systematically include other processes and periods. This is crucial to gaining insight into how local sources of moisture and their convective dynamics interact with the long-range transport of moisture from the Atlantic Ocean and land. Four processes will demand our attention. First, the role of the canopy in controlling the diurnal canopy-top fluxes of energy and carbon will require finer spatial resolution to explicitly resolve the radiative transfer and energy partitioning in the canopy and to determine how turbulence is modified at the canopy-atmosphere interface. Second, these canopy responses to the atmosphere should also be accompanied by improvements to the representation of how the entire plant respond to shading, water supply from the root zone, and canopy structure. Third, due to the key role played by the partitioning of direct and diffuse radiation by clouds and penetrating the rainforest canopy, it will be necessary to investigate how three-dimensional radiative effects modify the surface fluxes and their subsequent impact on turbulence and cloud dynamics. Though the use of such three-dimensional radiative models is computationally intensive, they could provide new insight into how dynamic heterogeneity (cloud shading) perturbs carbon and cloud cycling on subdaily and subkilometer scales. Lastly, the numerical experiments will have to include more detailed microphysical representations, which need to be related to the presence of aerosols. In brief, these processes (a) modify the optical properties involved in the transfer of radiation that influence relevant processes at the surface such as photosynthesis, plant transpiration, and the formation or advection of the morning low clouds above the canopy and (b) interact with cloud and rain drop formation. In controlling the gas-aerosol formation, we will need to take into account the active role played by chemistry in the formation of secondary organic aerosols, as well as perturbations caused by anthropogenic aerosols. These topics will be considered in the future version of the global weather model IFS.

Finally, the explicit and systematic numerical experiments by DALES, based on first principles that solve the meteorological and diurnal carbon cycle variables, and supported by detailed observations and by IFS results, are central to the development of a better understanding and representation of the interacting and dynamic systems of the Amazonian tropical rainforest on diurnal scales.

Appendix A: Physical and Biochemical Processes Included in the Numerical Experiment

A1. LES Numerical Experiment Configuration

The numerical experiments presented in this study can be reproduced by using the large-eddy simulation DALES. In Table A1, we present all the processes included in the experiments and their representation. Table A2 shows the initial conditions of the thermodynamic state variables and carbon dioxide. Tables A3 and A4 include all the surface conditions and the constants used in the photosynthesis-conductance model A-gs.

Table A1
List of Processes and Their Numerical Techniques Included in the Numerical Experiment of the Diurnal Variability in September 2014

Variables/process	Model technique
Radiation	One-dimensional RRTMG (Pedruzo-Bagazgoitia et al., 2017)
Thermodynamics and dynamics	Large-eddy simulation (Heus et al., 2010)
Microphysics	All-or-nothing (condensatin occurs if q mean state becomes saturated) (Heus et al., 2010)
CO_2 assimilation/Stomatal aperture	A-gs (Pedruzo-Bagazgoitia et al., 2017; Ronda et al., 2001)
Radiation/Stomatal aperture	Two-big leaves:sunlit/shaded (Pedruzo-Bagazgoitia et al., 2017; Ronda et al., 2001)
Surface (canopy top) fluxes	Penman-Monteith constrained by surface energy balance (Heus et al., 2010)
Soil flux	Four-layer restore (Heus et al., 2010)
Gas phase chemistry	BVOC-NO_x-O_3 mechanism (Ouwersloot et al., 2011)

Table A2
LES Configuration: Numerical Setting and Initial Thermodynamic Profiles

Domain	
Horizontal, (L_x, L_y)	(19,080, 19,080) m
Vertical, L_z	3,990 m
Grid points, (N_x, N_y)	(360, 360)
Grid points, N_z	200
Resolution $(\Delta x, \Delta y, \Delta z)$	(53, 53, 20) m
Horizontal numerical scheme state variables	Fifth order
Vertical numerical scheme state variables	Second order
Numerical scheme atmospheric constituent	κ scheme
Boundary conditions	
Horizontal	Periodic
Upper	Sponge layer
Lower	Coupled land surface model (see Tables A3 and A4)
Time integration	
Time step, dt	variable, set by CFL criterion with maximum value 1 s
Integration time	43,200 s
Averaging time statistics	300 s
Initial conditions	
Wind profile	
0 m < z < 3,990 m	$(u, v) = (-7, 1)$ m s^{-1}
Subgrid turbulent kinetic energy profile	
0 m < z < 90 m	TKE = 1.0 m^2 s^{-2}
90 m < z < 110 m	TKE = 0.5 m^2 s^{-2}
110 m < z < 3,990 m	TKE = 0.0 m^2 s^{-2}
Potential temperature profile	
0 m < z < 50 m	θ = 297 K
50 m < z < 3,990 m	$\theta = 297 + 1.29\ 10^{-1} \cdot$ (z 00- 50) K
Specific humidity profile	
0 m < z < 130 m	q = 16.6 $g_w\ kg_a^{-1}$
130 m < z < 3,990 m	q = 16.6 - 3. $10^{-3} \cdot$ (z − 130) $g_w\ kg_a^{-1}$
Carbon dioxide profile	
0 m < z < 110 m	CO_2 = 436 ppm
110 m < z < 170 m	CO_2 = 425 ppm
170 m < z < 290 m	CO_2 = 420 ppm
290 m < z < 450 m	CO_2 = 413 ppm
450 m < z < 550 m	CO_2 = 408 ppm
550 m < z < 3,990 m	CO_2 = 394 ppm

Note. Units specific moisture: grams water (g_w) per kilogram air (kg_a).

Table A3
Initial and Boundary Conditions Prescribed in the CONTROL DALES Numerical Experiment

Geographic coordinates for radiation	
Latitude (degree)	−2.6091
Longitude (degree)	−60.2093
Julian day	253
Starting hour simulation	10 UTC (06 LT)
Roughness length momentum (z_{om})	0.5 m
Roughness length heat (z_{oh})	0.1 m
Surface properties	A-gs model (see Table A4)
	Tropical forest
	Sandy loam
Initial surface temperature (T_s)	290 K
Albedo	0.15
Skin conductivity	0.
Vegetation cover	0.9
Leaf area index	5
Soil properties	
Temperature soil layer 1 (T_{soil1})	294 K
Temperature soil layer 2 (T_{soil2})	294 K
Temperature soil layer 3 (T_{soil3})	295 K
Temperature soil layer 4 (T_{soil4})	296 K
Temperature soil deep layer (T_{deep})	297 K
Volumetric soil moisture content soil layer 1 (W_{soil1})	0.3 m^3 m^{-3}
Volumetric soil moisture content soil layer 2 (W_{soil2})	0.3 m^3 m^{-3}
Volumetric soil moisture content soil layer 3 (W_{soil3})	0.3 m^3 m^{-3}
Volumetric soil moisture content soil layer 4 (W_{soil4})	0.3 m^3 m^{-3}
Volumetric content wilting point (W_{fc})	0.171 m^3 m^{-3}
Volumetric content field capacity (W_{fc})	0.4 m^3 m^{-3}
Saturated water volumetric water (W_{sat})	0.5 m^3 m^{-3}
Skin conductivity	40. W m^{-2} K^{-1}

Table A4
Values of the Parameters Used in the Plant Physiological and CO_2 Soil Efflux Models Are From, Respectively, Ronda et al. (2001), Lloyd and Taylor (1994) and Vilà-Guerau de Arellano et al. (2015)

Plant type	Parameter	(T = 298 K)	Q_{10}	T_1(K)	T_2(K)
C3	a_d (kPa^{-1})	0.07			
	α_o (mg J^{-1})	0.017			
	f_o (−)	0.89			
	K_x (m_{ground} m^{-1}_{leaf})	0.7			
	Γ (mg m^{-3}))	$68.5\rho_a$	1.5		
	g_{m298} (mm s^{-1})	7.0	2.0	278	301
	$A_{m,max}$(mg m^{-2} s^{-1})	2.2	2.0	281	311
	$g_{min,c}$(m s^{-1})	$2.5{\cdot}10^{-4}$			
Soil	Parameter				
	R10	0.15			
	Eact0	53.3 10^3			

Appendix B: Relating Incoming Shortwave Radiation and PAR

Figure B1 shows the incoming shortwave radiation and the photosynthetic active radiation (PAR) for 10 September 2014 measured above the canopy. It complements Figure 5 that shows the monthly average observations of the net available radiation. It also shows that as a first-order approximation PAR can be represented as 0.5 of the incoming shortwave radiation.

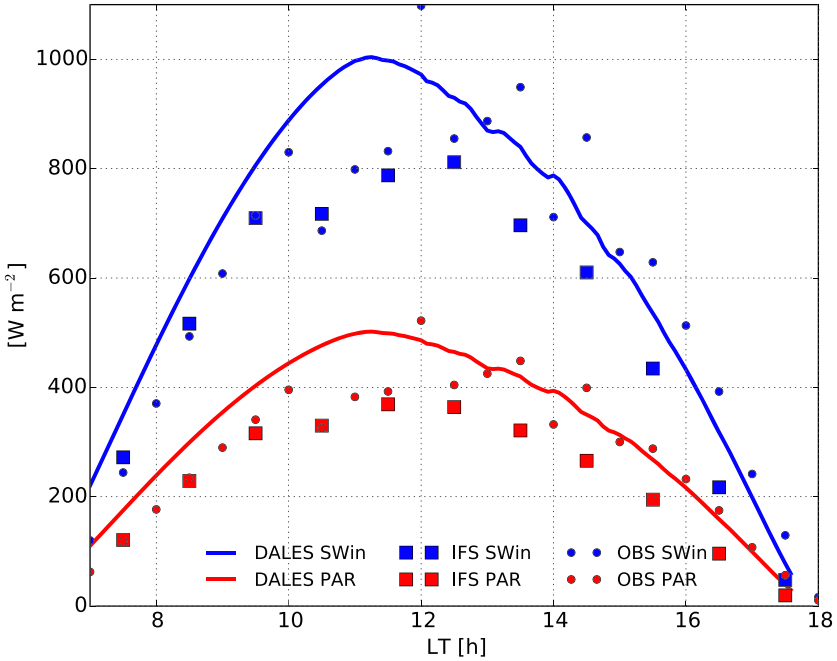

Figure B1. Evolution of the incoming shortwave radiation and the photo synthetically active radiation of 10 September 2014.

Appendix C: Thermodynamic Conditions During Dissipation of Shallow Cumuli

We present additional information on the thermodynamic variables of the dissipation of shallow cumuli (at 23.30 UTC or 19.30 LT) (Figures C1 and C2).

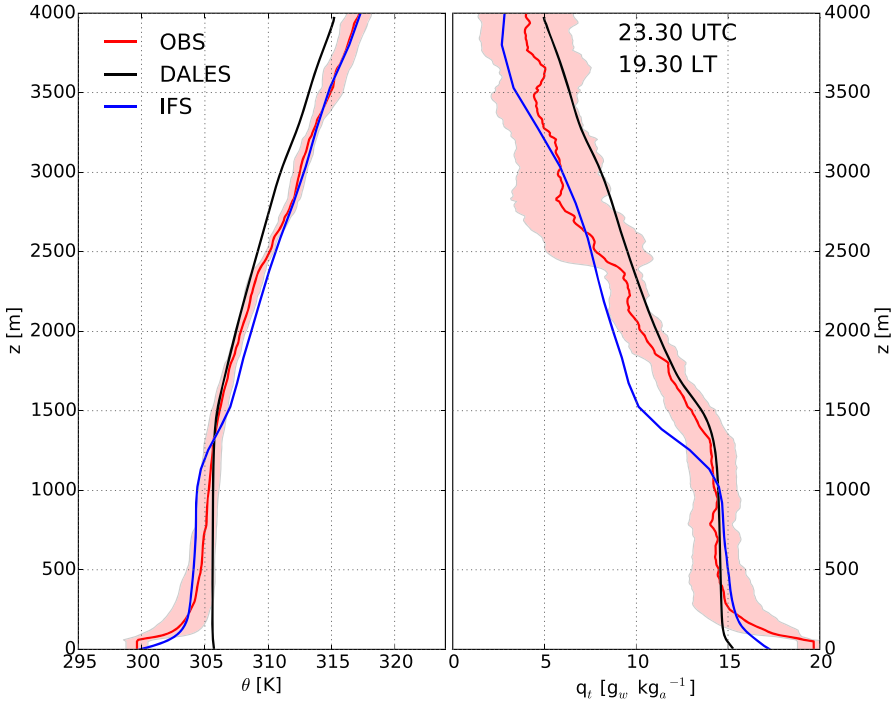

Figure C1. Same as Figure 10 but at 19.30 LT.

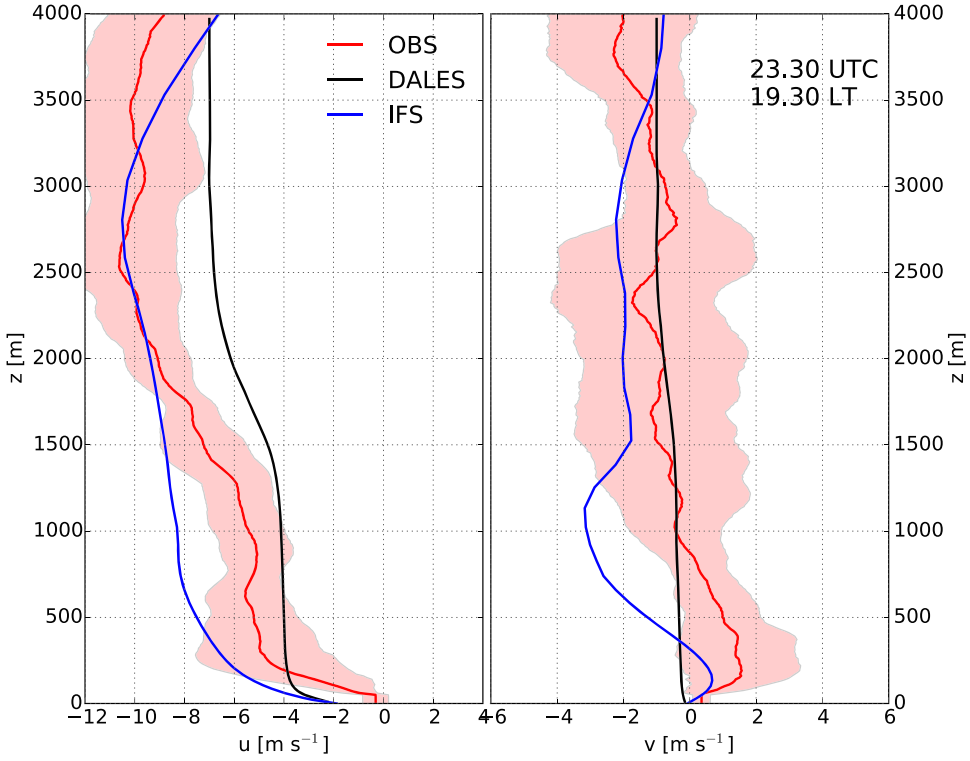

Figure C2. Same as Figure 11 but at 19.30 LT.

Appendix D: Flux Profiles of Heat, Moisture, and Carbon Dioxide

Figure D1 shows the temporal evolution of the vertical flux profiles for: liquid water potential temperature (a), buoyancy (b), the total specific humidity and the liquid water (c), and the carbon dioxide (d). At 10 LT, the atmospheric boundary layer is still cloudless. At 12 and 14 LT shallow cumuli are already active.

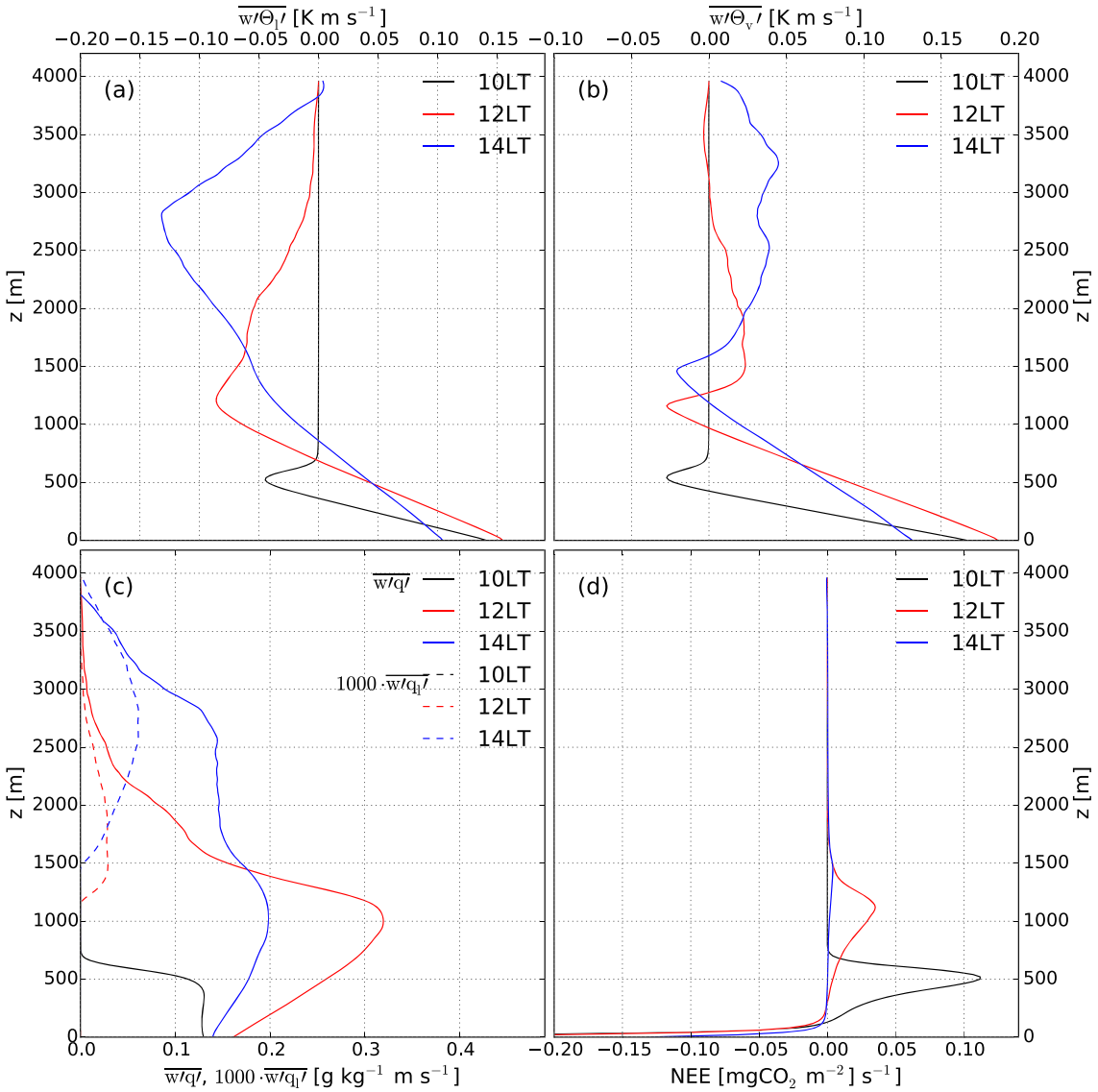

Figure D1. Kinematic vertical flux profile of (a) liquid water potential temperature, (b) potential temperature, (c) total specific humidity and liquid water content, and (d) carbon dioxide. The profiles are calculating first by doing an horizontal average on the three-dimensional DALES results and then average over 10 min.

Acknowledgments
The Atmospheric Radiation Facility (ARM), supported by the U.S. Department of Energy, Office of Science Biological and Environmental Research, is acknowledged for its financial and technical support in collecting the data during the GoAmazon2014/15 observations. The data sets used in this study were collected under scientific license 001030/2012-4 of the Brazilian National Council for Scientific and Technological Development (CNPq). J. D. F. acknowledges support from the U.S. Department of Energy (DOE) to participate in the GoAmazon2014/5 project (Grant SC0011075). We would like to thank two anonymous reviewers for their suggestions that have contributed to improving the paper. To ensure the reproducibility of the results and enable this case to be used as a benchmark, the DALES code, numerical settings and results, and the IFS results and observations are placed in http://doi.org/10.5281/zenodo.3759193 (GOAMAZON2014).

References

Agustí-Panareda, A., Diamantakis, M., Massart, S., Chevallier, F., Munoz-Sabater, J., Barré, J., & Wunch, D. (2019). Modelling CO_2 weather why horizontal resolution matters. *Atmospheric Chemistry and Physics*, *19*, 7347–7376. https://doi.org/10.5194/acp-2019-177

Agustí-Panareda, A., Massart, S., Chevallier, F., Boussetta, S., Balsamo, G., Beljaars, A., & Wunch, D. (2014). Forecasting global atmospheric CO_2. *Atmospheric Chemistry and Physics*, *14*, 11,959–11,983.

Anber, U., Gentine, P., Wang, S., & Sobel, A. H. (2015). Fog and rain in the Amazon. *Proceedings National Academy of Sciences*, *37*, 11,473–11,477.

Balsamo, G., Boussetta, S., Dutra, E., Beljaars, A., Viterbo, P., & Van den Hurk, B. (2011). The role of roughness sublayer dynamics within surface exchanges schemes. *ECMWF Newsletter*, *127*, 17–22.

Boussetta, S., Balsamo, G., Beljaars, A., Panareda, A.-A., Calvet, J.-C., Jacobs, C., et al. (2013). Natural land carbon dioxide exchanges in the ECMWF integrated forecasting system: Implementation and offline validation. *Journal of Geophysical Research: Atmospheres*, *118*, 5923–5946. https://doi.org/10.1002/jgrd.50488

Brown, A. R., Cederwall, R. T., Chlond, A., Duynkerke, P. G., Golaz, J., Khairoutdinov, M., & Stevens, B. (2002). Large-eddy simulation of the diurnal cycle of shallow cumulus convection over land. *Quarterly Journal of the Royal Meteorological Society*, *128*, 1075–1093. https://doi.org/10.1256/003590002320373210

Browning, K. A. (1993). The GEWEX Cloud System Study (GCSS). *Bulletin of the American Meteorological Society*, *74*, 387–399.

Buizza, R., Balsamo, G., & Haiden, T. (2018). IFS brings more seamless coupled forecasts. In *ECMWF Newsletter* (Vol.156, pp. 18–22). Reading, UK: ECMWF. https://www.ecmwf.int/en/newsletter/156/meteorology/ifs-upgrade-brings-more-seamless-coupled-forecasts

Burleyson, C. D., Feng, Z., Hagos, S. M., Fast, J., Machado, L. A. T., & Martin, S. T. (2016). Spatial variability of the background diurnal cycle of deep convection around the GoAmazon2014/5 field campaign sites. *Journal of Applied Meteorology and Climatology*, *55*(7), 1579–1598. https://doi.org/10.1175/JAMC-D-15-0229.1

Calvet, J. C. (2000). Investigating soil and atmospheric plant water stress using physiological and micrometeorological data. *Agricultural and Forest Meteorology*, *103*, 229–247.

Calvet, J. C., Noilhan, J., Roujean, J. L., Bessemoulin, P., Cabelguenne, M., Olioso, A., & Wigneron, J. P. (1998). An interactive vegetation SVAT model tested against data from six contrasting sites. *Agricultural and Forest Meteorology*, *92*, 73–95.

Cecchini, M. A., Machado, L. A. T., Wendisch, M., Costa, A., Krämer, M., Andreae, M. O., & Weinzierl, B. (2017). Illustration of microphysical processes in Amazonian deep convective clouds in the gamma phase space: Introduction and potential applications. *Atmospheric Chemistry and Physics*, *17*, 14,727–14,746. https://doi.org/10.5194/acp-17-14727-2017

Clothiaux, E. E., Ackerman, T. P., Mace, G. G., Moran, K. P., Marchand, R. T., Miller, M. A., & Martner, B. E. (2000). Objective determination of cloud heights and radar reflectivities using a combination of active remote sensors at the ARM CART sites. *Journal of Applied Meteorology*, *39*(5), 645–665. https://doi.org/10.1175/1520-0450(2000)039<0645:ODOCHA>2.0.CO;2

DoffSota, E., Meir, P., Malhi, Y., Nobre, A. D., Hodnett, M., & Grace, J. (2004). Soil CO_2 efflux in a tropical forest in the central Amazon. *Global Change Biology*, *10*, 601–617.

dos Michiles, A. A., & Santos Gielow, R., (2008). Above-ground thermal energy storage rates, trunk heat fluxes and surface energy balance in a central Amazonina forest. *Agricultural and Forest Meteorology*, *148*, 917–930.

Doughty, C. E., Goulden, M. L., Miller, S. D., & da Rocha, H. R. (2006). Circadian rhythms constrain leaf and canopy gas exchange in an Amazonian forest. *Geophysical Research Letters*, *33*, L15404. https://doi.org/10.1029/2006GL026750

Doutriaux-Boucher, M., Webb, M. J., Gregory, J. M., & Boucher, O. (2009). Carbon dioxide induced stomatal closure increases radiative forcing via a rapid reduction in low cloud. *Geophysical Research Letters*, *36*, L02703. https://doi.org/10.1029/2008GL036273

Feingold, G., Jiang, H., & Harrington, J. Y. (2005). On smoke suppresion of clouds in Amazonia. *Geophysical Research Letters*, *32*, L02804. https://doi.org/10.1029/2004GL021369

Finnigan, J. J., Shaw, R. H., & Patton, E. G. (2009). Turbulence structure above a vegetation canopy. *Journal of Fluid Mechanics*, *637*, 387–424.

Fitzjarrald, D. R., Moore, K. E., Cabral, O. M. R., Scolar, J., Manzi, A. O., & de Abreu Sá, D. (1990). Daytime turbulent exchange between the Amazon forest and the atmosphere. *Journal of Geophysical Research*, *95*(D10), 16,825–16,838. https://doi.org/10.1029/JD095iD10p16825

Foken, T. (2008). The energy balance closure problem: An overview. *Ecological Applications*, *18*, 1351–1367.

Freire, L. S., Gerken, T., Ruiz-Plancarte, J., Wei, D., Fuentes, J. D., Katul, G. G., & Chamecki, M. (2017). Turbulent mixing and removal of ozone within an Amazon rainforest canopy. *Journal of Geophysical Research: Atmospheres*, *122*, 2791–2811. https://doi.org/10.1002/2016JD026009

Fu, Z., Gerken, T., Bromley, G., Araújo, A., Bonal, D., Burban, B., & Stoy, P. C. (2018). The surface-atmosphere exchange of carbon dioxide in tropical rainforests: Sensitivity to environmental drivers and flux measurement methodology. *Agricultural and Forest Meteorology*, *263*, 292–307. https://doi.org/10.1016/j.agrformet.2018.09.001

Fuentes, J. D., Chamecki, M., Nascimento dos Santos, R. M., Von Randow, C., Stoy, P. C., Katul, G., et al. (2016). Linking meteorology, turbulence, and air chemistry in the Amazon Rain Forest. *Bulletin of the American Meteorological Society*, *97*(12), 2329–2342. https://doi.org/10.1175/BAMS-D-15-00152.1

Garstang, M., & Fitzjarrald, D. R. (1999). *Observations of surface to the atmosphere interactions in the tropics* (405 pp.). Oxford, UK: Oxford University Press.

Gentine, P., Holtslag, A. A. M., D'Andrea, F., & Ek, M. (2013). Surface and atmospheric controls on the onset of moist convection over land. *Journal of Hydrometeorology*, *14*, 1443–1462.

Gentine, P., Massmann, A., Linter, B. R., Alemhammad, S. H., Fu, R., Green, J. K., & Vilá-Guerau de Arellano, J. (2019). Land-atmosphere intercations in the tropics. *Hydrology and Earth System Sciences*, *23*, 4171–4197.

Gerken, T., Chamecki, M., & Fuentes, J. D. (2017). Air-parcels residence times within forest canopies. *Boundary-Layer Meteorology*, *165*, 29–54. https://doi.org/10.1007/s10546-107-0269-7

Gerken, T., Ruddell, B. L., Fuentes, J. D., Araujo, A., Brunsell, N. A., Maia, J., & Stoy, P. C. (2018). Investigating the mechanisms responsible for the lack of surface energy balance closure in a central Amazonian tropical rainforest. *Agricultural and Forest Meteorology*, *255*, 92–103.

Giambelluca, T. W., Hölscher, D., Bastons, T. X., Frazao, R. R., Nullet, M. A., & Ziegler, A. D. (1997). Observations of albedo and radiation balance over postforest land surfaces in the Eastern Amazon Basin. *Journal of Climate*, *10*, 919–928.

Giangrande, S. E., Feng, Z., Jensen, M. P., Comstock, J. M., Johnson, K. L., Toto, T., & Martin, S. T. (2017). Cloud characteristics, thermodynamic controls and radiative impacts during the Observations and Modeling of the Green Ocean Amazon (GoAmazon2014/5) experiment. *Atmospheric Chemistry and Physics*, *17*(23), 14,519–14,541. https://doi.org/10.5194/acp-17-14519-2017

Harman, I. N. (2012). The role of roughness sublayer dynamics within surface exchanges schemes. *Boundary-Layer Meteorology*, *142*, 1–20.

Heus, T., van Heerwaarden, C. C., Jonker, H. J. J., Siebesma, A. P., Axelsen, S., van den Dries, K., & Vilà-Guerau de Arellano, J. (2010). Formulation and numerical studies by the Dutch Atmospheric Large-Eddy Simulation (DALES). *Geoscientific Model Development*, *3*, 415–444.

Horn, G. L., Ouwersloot, H. G., Vilà-Guerau de Arellano, J., & Sikma, M. (2015). Cloud shading effects on characteristic boundary-layer lenght scales. *Boundary-Layer Meteorology*, *157*, 237–263.

Iacono, M. J., Delamere, J. S., Mlawer, E. J., Shephard, M. W., Clough, S. A., & Collins, W. D. (2008). Radiative forcing by long-lived greenhouse gases: Calculations with the AER radiative transfer models. *Journal of Geophysical Research*, *113*, D13103. https://doi.org/10.1029/2008JD009944

Jacobs, C. M. J., & de Bruin, H. A. R. (1997). Predicting regional transpiration of elevated atmospheric CO_2: Influence of the PBL-vegetation interaction. *Journal of Applied Meteorology*, *36*, 1663–1675.

Jacobs, A. G. F., Heusinkveld, B. G., & Holtslag, A. A. M. (2007). Seasonal and interannual variability of carbon dioxide and water balance over a grassland. *Climatic Change*, *82*, 163–177.

Jakub, F., & Mayer, B. (2017). The role of 1-D and 3-D radiative heating in the organization of shallow cumulus convection and the formation of cloud streets. *Atmospheric Chemistry and Physics*, *17*, 13,317–13,327.

Katul, G. G., Oren, R., Manzoni, S., & Higgins, C. (2012). Evapotranspiration: A process driving mass transport and energy exchange in the soil-plant-atmosphere-climate system. *Reviews of Geophysics*, *50*, RG3002.

Le Quéré, C., Raupach, M., Canadell, J. G., Marland, G., Bopp, L., Ciais, P., & Woodward, I. (2009). Trends in the sources and sinks of carbon dioxide. *Nature Geoscience*, *2*, 831–836. https://doi.org/10.1038/ngeo689

Lenderink, G., Siebesma, A. P., Cheinet, S., Irons, S., Jones, C. G., Marquet, P., & Soares, P. M. M. (2004). The diurnal cycle of shallow cumulus clouds over land. A single-column model intercomparison study. *Quarterly Journal of the Royal Meteorological Society*, *130*, 3339–3364.

Lin, C., Gentine, P., Frankenberg, C., Zhou, S., Kennedy, D., & Li, X. (2019). Evaluation and mechanism exploration of the diurnal hysteresis of ecosystem fluxes. *Agricultural and Forest Meteorology*, *278*, 107,642. https://doi.org/10.1016/j.agrformet.2019.107642

Lloyd, J., & Taylor, J. A. (1994). On the temperature dependence of soil respiration. *Functional Ecology*, *8*, 315–323.

Machado, L. A. T. (2000). The Amazon energy budget using the ABLE-2B and FluAmazon data. *Journal of the Atmospheric Sciences*, *57*(18), 3131–3144. https://doi.org/10.1175/1520-0469(2000)057<3131:TAEBUT>2.0.CO;2

Makarieva, A. M., Gorshkov, V. G., Sheil, D., Nobre, A. D., Bunyard, P., & Li, B. L. (2014). Why does air passage over forest yield more rain? Examining the coupling between rainfall, pressure, and atmospheric moisture content. *Journal of. Hydrometeorology*, *15*, 411–426.

Malhi, Y., Nobre, A. D., Grace, J., Kruijt, B., Pereira, M. G. P., Culf, A., & Scot, S. (1998). Carbon dioxide transfer over a Central Amazonina rain forest. *Journal of Geophysical Research*, *103*, 31,593–31,612.

Martin, S. T., Artaxo, P., Machado, L. A. T., Manzi, A. O., Souza, R. A. F., Schumacher, C., & Wendisch, M. (2016). Introduction: Observations and modeling of the Green Ocean Amazon (GoAmazon2014/5). *Atmospheric Chemistry and Physics*, *16*(8), 4785–4797. https://doi.org/10.5194/acp-16-4785-2016

Martin, C. L., Fitzjarrald, D., Garstang, M., Oliveira, A. P., Greco, S., & Brodwell, E. (1988). Structure and growth of the mixing layer over the Amazonian rain forest. *Journal of Geophysical Research*, *93*, 1361–1375.

Ouwersloot, H. G., de Arellano, J. V., van Stratum, B. J. H., Krol, M. C., & Lelieveld, J. (2013). Quantifying the transport of subcloud layer reactants by shallow cumulus clouds over the Amazon. *Journal of Geophysical Research: Atmospheres*, *118*, 13,041–13,059. https://doi.org/10.1002/2013JD020431

Ouwersloot, H. G., Moene, A. F., Attema, J. J., & Vilà-Guerau de Arellano, J. (2016). Large-eddy simulation comparison of neutral flow over a canopy: Sensitivity to physical and numerical conditions, and similarity to other representations. *Boundary-Layer Meteorology*, *162*, 71–89. https://doi.org/10.1007/s10546-016-0182-5

Ouwersloot, H. G., Vilà-Guerau de Arellano, J., van Heerwaarden, C. C., Ganzeveld, L. N., Krol, M. C., & Lelieveld, J. (2011). On the segregation of chemical species in a clear boundary layer over heterogenous surfaces. *Atmospheric Chemistry and Physics*, *11*, 10,681–10,704.

Patton, E. G., Sullivan, P. P., & Davis, K. J. (2003). The influence of a forest canopy on top-down and bottom-up diffusion in the planetray boundary layer. *Quarterly Journal of the Royal Meteorological Society*, *129*, 1415–1434.

Pedruzo-Bagazgoitia, X., Jiménez, P., Dudhia, J., & Vilà-Guerau de Arellano, J. (2019). Shallow cumulus representation and its interaction with radiation and surface at the convection grey zone. *Monthly Weather Review*, *147*, 2467–2483.

Pedruzo-Bagazgoitia, X., Ouwersloot, H. G., Sikma, M., van Heerwaarden, C. C., Jacobs, C. M. J., & Vilà-Guerau de Arellano, J. (2017). Direct and diffuse radiation in the shallow cumulus-vegetation system: Enhanced and decreased evapotranspiration regimes. *Journal of Hydrometeorology*, *18*, 1731–1748.

Ronda, R. J., de Bruin, H. A. R., & Holtslag, A. A. M. (2001). Representation of the canopy conductance in modeling the surface energy budget for low vegetation. *Journal of Applied Meteorology*, *40*, 1431–1444.

Schneider, T., Teixeira, J., Bretherton, C. S., Brient, F., Pressel, K. G., Scär, C., & Siebesma, A. P. (2017). Climate goals and computing the future of clouds. *Nature Climate Change*, *7*, 3–5.

Siebesma, A. P., Bretherton, C. S., Brown, A., Chlond, A., Cuxart, J., Duynkerke, P. G., & Stevens, D. E. (2003). A large eddy simulation intercomparison study of shallow cumulus convection. *Journal of the Atmospheric Sciences*, *60*(10), 1201–1219.

Sikma, M., Ouwersloot, H. G., Pedruzo-Bagazgoitia, X., van Heerwaarden, C. C., & Vilà-Guerau de Arellano, J. (2018). Interactions between vegetation, atmospheric turbulence and clouds under a wide range of background wind conditions. *Agricultural and Forest Meteorology*, *255*, 31–43.

Sikma, M., & Vilà-Guerau de Arellano, J. (2019). Substantial reductions in cloud cover and moisture transport by dynamic plant responses. *Geophysical Research Letters*, *46*, 1870–1878. https://doi.org/10.1029/2018GL081236

Spracklen, D. V., Arnold, S. R., & Taylor, C. M. (2012). observations of increases tropical rainfall preceded by air passage over forests. *Nature*, *489*, 282–285.

Twine, T., Kustas, W., Norman, J., Cook, D., Houser, P., Meyers, T., & Wesely, M. (2000). Correcting eddy-covariance flux underestimates over a grassland. *Agricultural and Forest Meteorology*, *103*(3), 279–300. https://doi.org/10.1016/S0168-1923(00)00123-4

van der Laan-Luijkx, I. T., van der Velde, I. R., Krol, M. C., Gatti, L. V., Domingues, L. G., Correia, C. S. C., & Peters, W. (2015). Response of the Amazon carbon balance to the 2010 drought derived with CarbonTracker South America. *Global Biogeochemical Cycles*, *29*, 1092–1108. https://doi.org/10.1002/2014GB005082

Vial, J., Dufresne, J. L., & Bony, S. (2013). On the interpretation of inter-model spread in CMIP5 climate sensitivity estimates. *Climatic Change*, *41*, 3391–3362.

Vilà-Guerau de Arellano, J., Gioli, B., Miglietta, F., Jonker, H., Baltink, H., Hutjes, R., & Holtslag, A. (2004). Entrainment process of carbon dioxide in the atmospheric boundary layer. *Journal of Geophysical Research*, *109*, D18110. https://doi.org/10.1029/2004JD004725

Vilà-Guerau de Arellano, J., van Heerwaarden, C. H., & Lelieveld, J. (2012). Modelled suppression of boundary-layer clouds by plants in a CO_2-rich atmosphere. *Nature Geosciences*, *5*, 701–704.

Vilà-Guerau de Arellano, J., van Heerwaarden, C. C., van Stratum, B. J. H., & van den Dries, K. (2015). *Atmospheric boundary layer: Integrating air chemistry and land interactions* (265 pp.). Cambridge, UK: Cambridge University Press.

von Randow, C., Manzi, A. O., Kruijt, B., de Oliveira, P. J., Zanchi, F. B., Silva, R. L., & Kabat, P. (2004). Comparative measurements and seasonal variations in energy and carbon exchange over forest and pasture in South West Amazonia. *Theoretical and Applied Climatology*, *78*, 5–26.

Wright, J. S., Fu, R., Worden, J. R., Chakraborty, S., Clinton, N. E., Risi, C., & Yin, L. (2017). Rainforest-initiated wet season onset over the southern Amazon. *Proceedings of the National Academy of Sciences*, *114*(32), 8481–8486. https://doi.org/10.1073/pnas.1621516114

Zelinka, M. D., Randall, D. A., Webb, M. J., & Klein, S. A. (2017). Clearing clouds of uncertainty. *Nature Climate Change*, *7*, 674–677.

Zhang, Y., & Klein, S. K. (2013). Factors controlling the vertical extent of fair-weather shallow cumulus clouds over land: Investigation of fiurnal-cycle observations collected at the ARM site. *Journal of the Atmospheric Sciences*, *70*, 1297–1315.

Zhuang, Y., Fu, R., Marengo, J. A., & Wang, H. (2017). Seasonal variation of shallow-to-deep convection transition and its link to the environmental condistions over the Central Amazon. *Journal of Geophysical Research: Atmospheres*, *122*, 2649–2666. https://doi.org/10.1002/2016JD025993